

Discovery and Characterization of a Highly Potent and Selective Aminopyrazoline-Based in vivo Probe (BAY-598) for the Protein Lysine Methyltransferase SMYD2

Erik Eggert, Roman C. Hillig, Silke Köhr, Detlef Stöckigt, Jörg Weiske, Naomi Barak, Jeffrey Mowat, Thomas Brumby, Clara D. Christ, Antonius ter Laak, Tina Lang, Amaury E. Fernández-Montalván, Volker Badock, Hilmar Weinmann, Ingo V. Hartung, Dalia Barsyte-Lovejoy, Magdalena Szewczyk, Steven Kennedy, Fengling Li, Masoud Vedadi, Peter J. Brown, Vijayaratnam Santhakumar, Cheryl H. Arrowsmith, Timo Stellfeld, and Carlo Stresemann

J. Med. Chem., **Just Accepted Manuscript** • DOI: 10.1021/acs.jmedchem.5b01890 • Publication Date (Web): 13 Apr 2016

Downloaded from <http://pubs.acs.org> on April 15, 2016

Just Accepted

“Just Accepted” manuscripts have been peer-reviewed and accepted for publication. They are posted online prior to technical editing, formatting for publication and author proofing. The American Chemical Society provides “Just Accepted” as a free service to the research community to expedite the dissemination of scientific material as soon as possible after acceptance. “Just Accepted” manuscripts appear in full in PDF format accompanied by an HTML abstract. “Just Accepted” manuscripts have been fully peer reviewed, but should not be considered the official version of record. They are accessible to all readers and citable by the Digital Object Identifier (DOI®). “Just Accepted” is an optional service offered to authors. Therefore, the “Just Accepted” Web site may not include all articles that will be published in the journal. After a manuscript is technically edited and formatted, it will be removed from the “Just Accepted” Web site and published as an ASAP article. Note that technical editing may introduce minor changes to the manuscript text and/or graphics which could affect content, and all legal disclaimers and ethical guidelines that apply to the journal pertain. ACS cannot be held responsible for errors or consequences arising from the use of information contained in these “Just Accepted” manuscripts.



Discovery and Characterization of a Highly Potent and Selective Aminopyrazoline-Based in vivo Probe (BAY-598) for the Protein Lysine Methyltransferase SMYD2

Erik Eggert,[†] Roman C. Hillig,[†] Silke Koehr,[†] Detlef Stöckigt,[†] Jörg Weiske,[†] Naomi Barak,[†] Jeffrey Mowat,[†] Thomas Brumby,[†] Clara D. Christ,[†] Antonius ter Laak,[†] Tina Lang,[†] Amaury E. Fernandez-Montalvan,[†] Volker Badock,[†] Hilmar Weinmann,[†] Ingo V. Hartung,[†] Dalia Barsyte-Lovejoy,[‡] Magdalena Szewczyk,[‡] Steven Kennedy,[‡] Fengling Li,[‡] Masoud Vedadi,^{‡,‡} Peter J. Brown,[‡] Vijayaratnam Santhakumar,[‡] Cheryl H. Arrowsmith,^{‡,§} Timo Stellfeld,^{*,†} and Carlo Stresemann^{†,*}

[†]Drug Discovery, Bayer AG, 13353 Berlin, Germany

[‡]Structural Genomics Consortium, University of Toronto, Toronto, ON, M5G 1L7

[#]Department of Pharmacology and Toxicology, University of Toronto, Toronto, ON, M5S 1A8.

[§]Princess Margaret Cancer Centre and Department of Medical Biophysics, University of Toronto, Toronto, ON, M5G 2M9.

ABSTRACT: Protein lysine methyltransferases have recently emerged as a new target class for the development of inhibitors that modulate gene transcription or signaling pathways. SET and MYND domain containing protein 2 (SMYD2) is a catalytic SET domain containing methyltransferase reported to monomethylate lysine residues on histone and non-histone proteins. Although several studies have uncovered an important role of SMYD2 in promoting cancer by protein methylation, the biology of SMYD2 is far from being fully understood. Utilization of highly potent and selective chemical probes for target validation has emerged as a concept which circumvents possible limitations of knockdown experiments and, in particular, could result in an improved exploration of drug targets with a complex underlying biology. Here, we report the development of a potent, selective and cell-active, substrate-competitive inhibitor of SMYD2, which is the first reported inhibitor suitable for in vivo target validation studies in rodents.

INTRODUCTION

SMYD2 is a catalytic SET domain containing protein methyltransferase reported to monomethylate lysine residues on histone and non-histone proteins.¹ SMYD2 has been proposed as a potential therapeutic target in cancer. Its overexpression has been reported in cancer cell lines as well as in esophageal squamous carcinoma (ESCC), bladder carcinoma, gastric cancer and pediatric acute lymphoblastic leukemia patients.²⁻⁶ In these studies, SMYD2 overexpression often correlated with lower survival rate and was suggested to be a clinically relevant prognostic marker. Knockdown of SMYD2 in overexpressing ESCC, bladder and gastric cancer cell line models significantly reduced cell proliferation.² Initially, SMYD2 was characterized as

1
2
3 methylating H3 lysine 36⁷ and lysine 4 when interacting with HSP90a.⁸ Methylation of histones
4
5 by SMYD2 has been connected to increased transcription of genes involved in cell-cycle
6
7 regulation, chromatin remodeling and transcriptional regulation.⁸ In addition, several studies
8
9 have uncovered an important role of SMYD2 methylation activity toward non-histone proteins
10
11 closely connected to cancer. This is in line with the emerging concept that posttranslational
12
13 methylation of non-histone proteins (e.g., of transcription factors) by protein methyltransferases
14
15 can also substantially alter protein function. Thereby, a regulatory role of lysine methylation can
16
17 probably be extended to multiple cellular pathways, besides transcriptional regulation and
18
19 histones.^{9,10} So far, the best-characterized example of SMYD2 methylation of a non-histone
20
21 protein is the tumor suppressor transcription factor p53.^{11–16} Transcriptional activity of p53 is
22
23 inhibited by SMYD2-mediated posttranslational methylation at lysine 370 (K370).^{13,17} The
24
25 structural basis of p53 methylation by SMYD2 has been characterized by solving the crystal
26
27 structure of a ternary complex with the cofactor product *S*-adenosylhomocysteine and a p53-
28
29 derived substrate peptide.¹⁶ It has been proposed that methylation at K370 reduces the DNA-
30
31 binding efficiency of p53 and subsequently prevents the transcriptional activation of p53 target
32
33 genes.¹³ In the same study, a knockdown of SMYD2 and treatment with doxorubicin led to an
34
35 increase in p53-mediated cell-cycle arrest and apoptosis. In line with these observations, low
36
37 SMYD2 gene expression was suggested as a predictive marker for an improved response to
38
39 neoadjuvant chemotherapy in breast cancer patients.¹⁸ Besides p53, several other proteins have
40
41 been identified as SMYD2 substrates, including the estrogen receptor (ER),^{19,20} PARP1,²¹
42
43 retinoblastoma protein (Rb)⁴ and HSP90.^{22,23} Mechanistically, methylation of HSP90 has been
44
45 connected to the normal physiological role of SMYD2 in muscle biology,^{24,25} as well as in
46
47 cancer.²³ These studies indicate that SMYD2 has many substrates and various potentially tissue-

specific physiological and pathogenic functions. SMYD2 therefore represents a very attractive target for further exploration in different disease-relevant models. Nevertheless, the biology of SMYD2 is still poorly understood, and the molecular contribution of individual substrates to specific knockdown phenotypes remains largely unknown. For a more unbiased interpretation of biological experiments, fully profiled chemical probes can substantially contribute to preclinical target validation.^{26,27} Although first cellular-active probe inhibitors of SMYD2 have been described (Figure 1), there is a need for structurally orthogonal chemical probes to enable cross-validation studies and thereby rule out unspecific effects.²⁶ The publication of **1** (AZ505)¹² was the first disclosure of a co-crystal structure of an inhibitor bound to SMYD2 and paved the way for further studies, leading to the discovery of **2** (LLY-507),²⁸ and **3** (A-893),²⁹ which have reported significantly improved potency. Analysis of the respective co-crystal structures reveals that all three inhibitors bind in a similar fashion, occupying the same binding pockets. Furthermore, the cellular activity of the known inhibitors is limited, and no data about in vivo applicability have been published. Here we report the discovery of a potent and selective aminopyrazoline-based small molecule inhibitor (*S*)-**4** (BAY-598).^{30,31} We show that (*S*)-**4** has a distinctly different binding mode compared to previous inhibitors, utilizing a dichlorophenyl moiety as so far unprecedented chemical motif for addressing the methyl-lysine binding pocket of SMYD2. For the first time we are presenting in vivo xenograft and DMPK data for a SMYD2 inhibitor. In addition to previously described inhibitors (*S*)-**4** shows very potent cellular activity combined with reasonable DMPK properties (Figure 1). Furthermore, we are indicating the potential that this inhibitor might offer to the field of protein methyltransferases in the quest to fully explore the underlying complex biology and therapeutic potential of SMYD2 by validating AHNAK protein³² as a new cellular substrate.

RESULTS AND DISCUSSION

The potential link between SMYD2 and cancer motivated us to screen the Bayer compound collection, with the aim of identifying small-molecule inhibitors of the enzyme. To this end, a scintillation proximity assay (SPA) was set up using recombinant His-tagged SMYD2, a biotinylated p53-derived peptide substrate and tritiated *S*-adenosyl-L-methionine (^3H -SAM) (Figure 2A). Of the three million compounds tested in a primary HTS, we identified more than 2300 confirmed hits which inhibited SMYD2 with IC_{50} values below 15 μM . Among the multiple structural clusters and singletons in the hit list, several offered starting points with low micromolar potency and tractable chemical matter, and our attention was drawn to pyrazolines such as compound **5**. Initial hits and later derivatives of the pyrazoline series showed stabilizing effects in an SMYD2 thermal shift assay (TSA) (Figure 2B). In addition, binding of compound **6** to SMYD2 was validated by isothermal titration calorimetry (ITC), which indicated a submicromolar binding constant ($K_d = 540 \text{ nM}$, Figure 2C) and a high enthalpic contribution to the binding energy. As the latter reduces the likelihood of nonspecific off-target activities, the ITC data underscored the attractiveness of pyrazoline hit **5**.^{33,34} It transpired that compounds of this structural series had been prepared during the course of an in-house program as antagonists for protease-activated receptor 1 (PAR1), a G-protein-coupled receptor which is highly expressed in platelets and plays an important role in thrombin signaling and platelet aggregation.^{35,36}

Chemistry. The pyrazoline compounds of interest were synthesized according to previously described procedures.³⁷ Synthesis of the required intermediates **10a–f** started from the commercially available 2-amino-1-phenylethanones **7** (Scheme 1). Protection of the amines as the allyl carbamates **8** was followed by Mannich reaction with formaldehyde and piperidine, and

the resulting product mixture was treated with hydrazine monohydrate to install the pyrazoline moiety (compounds **9**). Subsequent reaction with diphenyl *N*-cyanocarbonimidate resulted in intermediates **10a–f**.

The synthesis of compounds **5**, **6** and **12–24** began with **10a** (Scheme 2). Treatment of **10a** with the respective aniline or amine provided intermediates **11a–i**. Deprotection to the 4-aminopyrazolines and further elaboration led to the desired amides **5**, **6** and **12–23** by a sequence of optional reductive N-alkylation, and amide formation. For the hydroxyacetyl derivatives **5**, **6**, and **12–21**, the amide was formed by using acetoxyacetyl chloride, followed by treatment of the crude amide with methanolic potassium carbonate to remove the acetyl moiety. The amino acid amide **22** was prepared by a coupling with 9-fluorenylmethoxycarbonyl (Fmoc) protected glycine (HATU, NMM, DMF), followed by removal of the Fmoc group with piperidine. Amide formation with methoxyacetylchloride gave compound **23**. Furthermore, oxoimidazolidine **24** was prepared by reaction of the N-unsubstituted 4-aminopyrazoline derivative with chloroacetyl chloride and treatment of the resulting chloroacetamide with urotropine.

Compounds **4** and **25–29** were prepared from intermediates **10b–f**, by the addition of 3-(difluoromethoxy)aniline, followed by installation of the N-ethylated hydroxyacetamide as described above (Scheme 3).

The synthesis of compounds **30–34** started from intermediate **10d** by addition of the respective aniline derivatives, followed by introduction of the N-ethylated hydroxyacetamide (Scheme 4).

Compounds **4**, **28** and **30–34** were separated into their enantiomers by preparative chiral HPLC or chiral Supercritical Fluid Chromatography. For compounds **6** and **4**, the integrity of the pyrazoline stereocenter was tested. The compounds were stable to racemization in aqueous

solution at pH 7, as well as in mouse and human plasma at 37 °C, for at least 48 hours. However, clean racemization was obtained under basic conditions and microwave irradiation (DBU, THF, 90 °C).

Structure–Activity Relationships. Our initial structure–activity relationship (SAR) studies of 3-(4-chlorophenyl)pyrazoline derivatives with respect to SMYD2 inhibition are summarized in Table 1. For the carboximidamide N-substituent (R^3), a meta-substituted phenyl seemed optimal, with the 3-(difluoromethoxy)phenyl derivative **6** displaying highest potency and binding efficiency³⁸ (IC_{50} = 0.8 μ M, BEI = 12.5). Small para substituents are tolerated, such as with the 3-chloro-4-fluorophenyl, 3,4-dichlorophenyl and 2,2-difluoro-1,3-benzodioxol-5-yl derivatives **5**, **12** and **13** (IC_{50} = 1.7, 3.3 and 2.2 μ M, respectively). In contrast, the 4-(difluoromethoxy)phenyl derivative **14** is more than 15-fold less active than the corresponding meta-derivative **6**. The extended 3-chlorophenethyl derivative **15** showed no measurable activity (IC_{50} > 20 μ M), implying that the space within the relevant binding pocket is limited. Non-aromatic derivatives, such as 4,4,4-trifluorobutyl-substituted **16** or the cyclopropylethyl derivative **18**, are less potent than **6** (IC_{50} = 6.9 and 8.3 μ M for **16** and **18**, respectively). Surprisingly, the corresponding *n*-butyl derivative **17** is inactive (IC_{50} > 20 μ M). The SAR for PAR1 antagonism at the carboximidamide N-substituent appears to be rather flat: all compounds **5**, **6** and **12–18** are potent PAR1 antagonists, with IC_{50} values below 100 nM.

With respect to the amide moiety, it became clear that the presence and orientation of a hydrogen-bond donor has a large impact on potency towards SMYD2 (Table 2). Variation of the amide *N*-alkyl substituents (R^1) revealed that the *N*-ethyl derivative is preferred: secondary amide **19** (IC_{50} = 10.9 μ M) is about 10-fold less active, and the *N*-propyl derivative **20** is also less potent, than the corresponding *N*-ethyl derivative **6** (IC_{50} = 0.8 μ M), whereas the larger

cyclopropylmethyl substituent in **21** resulted in a loss of potency ($IC_{50} > 20 \mu M$). Replacement of the hydroxyacetyl in compound **12** ($IC_{50} = 3.3 \mu M$) by an aminoacetyl group gave the equipotent derivative **22** ($IC_{50} = 2.8 \mu M$). In contrast, the methoxyacetyl derivative **23**, lacking the hydrogen-bond donor, is inactive ($IC_{50} > 20 \mu M$). In compound **24**, where the hydrogen-bond donor is fixed in an oxoimidazolidine ring, there is significantly reduced potency ($IC_{50} = 6 \mu M$) relative to the *N*-ethyl derivative **6**. Based on the available amide derivatives, with BEI values in the same range (10 to 11), an improvement in the binding efficiency was not envisaged. Furthermore, alterations of the amide moiety did not offer a path forward to selectivity against PAR1. Compounds **22**, **23** and **24** are in a similar potency range for PAR1 antagonism, and greater than 10-fold more potent against PAR1 ($IC_{50} = 130, 30$ and 100 nM, respectively) than SMYD2.

At this stage, we selected compound **6** for co-crystal structure determination with SMYD2, based on its potency and promising biophysical properties. Compound **6** was soaked into crystals of SMYD2 grown in the presence of SAM. The crystal structure revealed that compound **6** binds into the substrate peptide binding pocket of SMYD2; the observed binding mode is consistent with the previously established SAR. There is a very good steric and electrostatic fit of **6** to the substrate binding site of SMYD2 (Figure 3A and 3B). The pyrazoline and the NH of the carboximidamide form hydrogen bonds to Gly183. The 4-chlorophenyl substituent inserts into the lysine binding channel and is engaged in π -stacking interactions with Phe184 and Tyr240. There is a good fit of the 3-(difluoromethoxy)phenyl substituent into the adjacent hydrophobic pocket-1, with the difluoromethoxy group pointing into a hydrophobic subpocket. Although racemic **6** was used for soaking, the density maps reveal that only the *S*-enantiomer is bound. The *S* configuration at the pyrazoline provides an optimal exit vector for the hydroxyacetamide

substituent, which occupies pocket-2 and forms two hydrogen bonds with Thr185 (Figure 3A). The *N'*-nitrile of the carboximidamide contributes to a water-bridged hydrogen bond with Ser196. Based on the crystal structure of compound **6**, we envisioned that further exploration of the aniline and amide moieties would not lead to a significant improvement of potency and binding efficiency. Therefore, we elected to focus on derivatives of the 4-chlorophenyl substituent, which were underrepresented in our compound library.

With the co-crystal structure in hand, we employed molecular modeling for the prioritization of derivatives. In particular, WaterMap calculations,^{39,40} which estimate the position and the thermodynamic properties of water molecules in the ligand-free structure, suggested the introduction of a second substituent at the 3-position of the 4-chlorophenyl group. To test this hypothesis, a few derivatives were synthesized (see Table 3). The unsubstituted phenyl derivative **25** is inactive, while the 4-bromo derivative **26** ($IC_{50} = 1.1 \mu M$) is as potent as the 4-chloro derivative **6**, indicating the importance of a hydrophobic substituent at the 4-position. As predicted by WaterMap calculations, introduction of a second substituent at the meta position, as exemplified by 3,4-dichloro derivative **4** ($IC_{50} = 0.08 \mu M$, BEI = 13.5) and 4-chloro-3-methyl derivative **28** ($IC_{50} = 0.08 \mu M$, BEI = 14), resulted in significantly improved potency (ca. 10-fold greater than **6**) and binding efficiency. As highlighted in Figure 3C, the two chloro substituents are co-located with two calculated water sites that have high free energy, suggesting an optimal water displacement by 3,4-dichlorophenyl and thus a lower binding free energy than for the 4-chlorophenyl or the unsubstituted phenyl derivative, consistent with the observed potency difference for these derivatives. However, introduction of a third substituent leads to a decrease in potency compared to the 3,4-disubstituted derivatives, as exemplified by 4-chloro-3,5-dimethyl derivative **27** ($IC_{50} = 0.57 \mu M$). Compound **29**, with the bulkier 1,3-benzodioxole

moiety, is also less potent ($IC_{50} = 4.2 \mu M$), suggesting that the SAR at this position is rather steep.

Compound **4** was selected for further biological and crystallographic studies. The co-crystal was obtained by soaking (*S*)-**4** into crystals of SAM-bound SMYD2. Structure determination revealed that (*S*)-**4** features an almost identical binding mode as compound **6**, as evidenced in the overlay of both structures (Figure 3D). In line with the observed *S* configuration of compound **6** and (*S*)-**4**, we observed a greater than 50-fold difference in the IC_{50} values of the two enantiomers of **4** [27 nM for (*S*)-**4** vs 1.7 μM for (*R*)-**4**, see Table 4]. Introduction of the additional 3-chloro substituent also resulted in a dramatic decrease in the antagonistic effect on PAR1 [$IC_{50} = 1.7 \mu M$ for (*S*)-**4** and $>30 \mu M$ for (*R*)-**4**]. Although (*S*)-**4** proved to be the active isomer for both SMYD2 inhibition and PAR1 antagonism, there is a greater than 50-fold selectivity for SMYD2 relative to PAR1.

The co-crystal structures of compound **6** and (*S*)-**4** revealed that the pyrazoline-based SMYD2 inhibitors feature a different binding mode to other recently reported inhibitors. Thus, **1**¹² and **2**²⁸ (Figure 4A) have published IC_{50} values of 0.12 μM and <15 nM, respectively, and like (*S*)-**4** they bind to the substrate binding site of SMYD2. The structures of the three inhibitors are superimposed in Figure 4B. All ligands occupy the lysine binding channel and the adjacent hydrophobic pocket-1; however, (*S*)-**4** employs pocket-2 via hydrogen-bond interactions with its hydroxyacetyl moiety (cf. Figure 2A), which are not present in **1** or **2**. **1** and **2**, on the other hand, occupy a remote hydrophobic pocket-3 which is not addressed by (*S*)-**4**. Figure 4C provides a view into the lysine binding channel (the respective motifs are highlighted in color on the structures in Figure 4A). **2** binds with its *N*-alkylpyrrolidine moiety at this position, which is structurally closely related to the lysine side chain of a methylated substrate peptide. **1** and (*S*)-**4**

address the lysine channel with aromatic substituents. Noteworthy, the 3,4-dichlorophenyl group of **1** and of (*S*)-**4** bind to different positions.

Based on 3,4-dichlorophenyl as a novel lysine channel binding motif, we identified several pyrazoline derivatives as potent SMYD2 inhibitors (see Table 4). Aiming to identify a candidate for in vivo experiments, we focused on the potent *S*-enantiomers of these derivatives, profiling them in pharmacokinetic assays in vitro. (*S*)-**4** showed moderate stability upon incubation with rat hepatocytes ($CL_{\text{blood}} = 2.5 \text{ L/h/kg}$), as well as moderate apparent permeability (34 nm/s) and a hint of active transport in the Caco2 assay (efflux ratio = 5). In comparison, the 4-chloro-3-methylphenyl derivative (*S*)-**28** had similar permeability and efflux (33 nm/s, efflux ratio = 7), and slightly lower metabolic stability in rat hepatocytes ($CL_{\text{blood}} = 2.8 \text{ L/h/kg}$). Compounds (*S*)-**30** and (*S*)-**32–34** exhibited high metabolic stability ($CL_{\text{blood}} = 1.8\text{--}0.3 \text{ L/h/kg}$); however, these derivatives have very low aqueous solubility (<5 mg/L), thereby limiting their suitability for in vivo experiments. On the other hand, the methoxyphenyl derivative (*S*)-**31** has high aqueous solubility (163 mg/L) and moderate permeability with a hint of active transport (62 nm/s, efflux ratio = 3) in the Caco2 assay; nevertheless, (*S*)-**31** displayed low stability upon incubation with rat hepatocytes ($CL_{\text{blood}} = 3.2 \text{ L/h/kg}$), and thus bioavailability is expected to be low. Based on these data, (*S*)-**4** was selected for further in vitro and in vivo studies. The in vivo pharmacokinetic properties of (*S*)-**4** were first evaluated by a single-dose administration of (*S*)-**4** at 0.4 mg/kg by i.v. bolus or 0.8 mg/kg p.o., respectively, to rats: there was moderate blood clearance (1.6 L/h/kg) and a low bioavailability of 24% (see Supporting Information Figure S1A). These data prompted us to assess the exposure of (*S*)-**4** following oral administration. Hence, we treated mice with 10–100 mg/kg po q.d. which are well tolerated doses of (*S*)-**4**. As a result, unbound IC_{50} [cellular methylation In-Cell Western (ICW) assay – see Figure 7A-C] is

covered for ~9 to ~12 hours at steady state when 10 and 100 mg/kg, respectively, are administered (see Supporting Information Figure S1B).

Potency, Selectivity and Inhibition Mode. (*S*)-4 showed potent *in vitro* inhibition of SMYD2 with an IC_{50} of 27 ± 7 nM in the biochemical SPA assay (Figure 5A). To analyze the mode of inhibition and affinity of (*S*)-4, our SMYD2 protein preparation was characterized with respect to its apparent Michaelis–Menten constants for SAM and the p53 peptide substrate (data not shown). The $K_{m(app)}$ values of 60 nM and 1 μ M, respectively, were in excellent agreement with the constants previously reported using a similar assay.¹² Then, we performed IC_{50} determinations at increasing concentrations of one substrate and a fixed amount of the other ($[S] = K_{m(app)}$), and applied the Cheng–Prusoff relationship⁴¹ as described elsewhere.⁴² Increasing the concentration of peptide substrate resulted in a linear increase in IC_{50} (Figure 4B, upper panel), as would be expected for a competitive mode of inhibition. Fitting these data to the corresponding Cheng–Prusoff competitive inhibition model revealed a $K_{i(app)}$ of 8 ± 1 nM (SD). On the other hand, when SAM concentrations were titrated to saturation, we observed a decrease in IC_{50} which converged to a constant value (Figure 4B, lower panel). This type of behavior toward SAM corresponds to an uncompetitive mode of inhibition. Consequently, the IC_{50} vs $[S]/K_{m(app)}$ plot fits best to the Cheng–Prusoff model for uncompetitive inhibition, yielding an inhibitor constant $\alpha Ki_{(app)}$ of 28 ± 3 nM (SD). Our data suggest that (*S*)-4 is a peptide-competitive, SAM-uncompetitive inhibitor of SMYD2 methyltransferase activity, which preferably binds to the SMYD2–SAM substrate complex. Interestingly, SMYD2 has been reported to follow a random sequential Bi Bi mechanism of substrate binding,^{12,17} but the uncompetitive mode of inhibition of (*S*)-4 regarding the SAM cofactor suggests an ordered sequential Bi Bi mode of substrate binding, where SAM would be required to bind before the

peptide substrate. Similar results have recently been described for inhibitors of the SAM-dependent arginine methyltransferase PRMT5.⁴³

For further evaluation of selectivity, (*S*)-**4** was tested on a panel of 32 additional methyltransferases, including closely related family members SMYD3, SUV420H1 and SUV420H2. As a result, (*S*)-**4** displayed >100-fold selectivity for SMYD2, with very weak residual activity toward the closest related methyltransferase SMYD3 (IC₅₀ ~3 μM) (Figure 5C). In addition to the methyltransferases, (*S*)-**4** was also profiled in the commercially available KINOMEScan (DiscoverX)⁴⁴ and LeadProfilingScreen (Eurofins Panlabs) assay panels to fully determine relative selectivity and specificity for kinases and other primary molecular targets, including several CNS targets. Overall, we were able to confirm the high selectivity and specificity of (*S*)-**4** for SMYD2 inhibition (see Supporting Information Tables S1 and S2).

Cellular Methylation Activity on p53.

The ability of (*S*)-**4** to inhibit SMYD2 was tested by monitoring its effects on cellular p53 methylation using different cellular mechanistic assays. First, we generated a polyclonal antibody (SY46) for the specific detection of p53 monomethylation at lysine 370, as described elsewhere.¹³ This antibody was then tested on recombinant p53 protein which had been in vitro methylated by SMYD2 in a western blot. Specificity for methylated p53 was confirmed by the exclusive detection of the in vitro methylated p53 protein isoforms, whereas the non-methylated p53 was not detected (Figure 6A). Endogenous methylation of p53 protein was characterized by treatment of KYSE-150 esophageal cancer cells with increasing concentrations of (*S*)-**4** for 5 days. The KYSE-150 cell line model was selected based on a described SMYD2 gene amplification² and a heterozygous R248Q mutation in p53 (COSMIC) leading to p53 protein

1
2
3 accumulation without a stress stimulus. After treatment with (*S*)-4, a significant reduction of
4
5 methylation was detected confirming that p53 is a cellular target of SMYD2-dependent
6
7 methylation (Figure 6B). Nevertheless overall endogenous detection of p53 protein methylation
8
9 led to weak signals, hence this method was not useful for the determination of a cellular IC₅₀.
10
11 Therefore, we additionally employed an established system with a transient FLAG-tagged
12
13 SMYD2 and FLAG-tagged p53 overexpression in HEK293T cells as benchmark assay. This
14
15 assay has been used previously to characterize the structurally unrelated SMYD2 inhibitor **2**.²⁸
16
17 As shown in Figure 6C, (*S*)-4 showed a concentration-dependent decrease in p53 methylation
18
19 without affecting p53 total protein levels. A cellular IC₅₀ of 58 nM was determined (Figure 6D),
20
21 which confirms that (*S*)-4 is the most potent cellular-active SMYD2 inhibitor known to date
22
23 (Figure 1).
24
25
26
27
28
29

30 **Characterization and Inhibition of SMYD2 Mediated AHNAK methylation**

31
32
33 To further characterize the effects of our aminopyrazoline-based inhibitors on the cellular
34
35 methylation activity of SMYD2, we generated a polyclonal cell line derived from KYSE-150
36
37 with stable N-terminal 2xc-myc-tagged SMYD2 overexpression to maximize cellular
38
39 methylation activity. In an immunofluorescence analysis, SMYD2 was localized mainly in the
40
41 cytosol (Supplementary Figure S2A), as reported by others.²² Surprisingly, the antibody SY46
42
43 directed against methylated p53 showed a very strong signal specifically in the clones with
44
45 SMYD2 overexpression in the immunochemistry staining not derived from p53 protein
46
47 (Supplementary Figure S2B-C). We validated the novel SMYD2 substrate giving rise to the
48
49 strong immunochemistry staining signal by knockdown and overexpression experiments in
50
51 additional cell lines to be derived from AHNAK protein³² (Figure 7B and Supplementary Figure
52
53 2D-F). AHNAK methylation has been very recently reported in a proteomics study by other as
54
55
56
57
58
59
60

an additional methylation substrate of SMYD2 further confirming our results.⁴⁵ Importantly, we used the strong AHNAK methylation signal to set up an In Cell Western (ICW) assay for cellular optimization of our lead series (Figure 7A). The methylation signal was reduced by treatment with increasing concentrations of (*S*)-**4**, derivatives of the aminopyrazoline series or **1** (Figure 7A). In addition (*S*)-**4** specifically reduced methylation of AHNAK without altering AHNAK protein expression in a western blot (Figure 7B). Importantly IC₅₀ values in the cellular ICW assay for aminopyrazolines correlated with potency in the scintillation proximity assay (Figure 7C), and were also comparable to the p53 methylation assay (see Figure 6D). Our results of the methylation of AHNAK and the recent identification of many additional methylation targets⁴⁵ clearly point towards additional roles beyond p53 regulation of SMYD2, and further studies supported by potent and selective inhibitors as (*S*)-**4** are needed to fully elucidate the underlying biology.

Characterization of (*S*)-**4** in Proliferation and Apoptosis Assays.

To explore the potential effects of (*S*)-**4** on proliferation, we tested a panel of 240 different cancer cell lines (OncoPanel 240/Eurofins Panlabs). Cell lines were long-term cultured with (*S*)-**4** for 10 days to allow for a sufficient translation of demethylation of SMYD2 substrates to potential antiproliferative effects, which takes 48–72 hours (Supplementary Figure S2C). (*S*)-**4** exposure resulted in only limited responses in a subset of cell lines: an antiproliferative response with IC₅₀ <10 μM was seen in 21 cell lines (~9%); however, most cell lines (83%) did not reach 50% proliferation inhibition with 20 μM of (*S*)-**4** (Figure 8A). In addition, there was no clear preference for a specific tissue origin of the responding cancer cell line. Thus, SMYD2 inhibition by (*S*)-**4** has only limited proliferation effects in a small subset of cancer cell lines under the employed conditions. Based on the observation that p53 protein is methylated by SMYD2, which

1
2
3 should lead to suppression of apoptosis, we were additionally interested in the effects of (S)-4 in
4
5 combination with an apoptotic stimulus. KYSE-150, U2OS and A2780 cell lines were pre-
6
7 treated with (S)-4 or inactive derivative **25** (see Table 3) for 2 days (demethylation phase),
8
9 followed by treatment with doxorubicin (apoptotic trigger). (S)-4, but not **25**, significantly
10
11 improved caspase 3/7 activation in all three tested cell lines without inducing apoptosis alone
12
13 (Figure 7B). Thus, SMYD2 inhibition can enhance apoptotic responses.
14
15
16
17

18 **The First Chemical Probe Suitable for In Vivo Characterization of SMYD2 Inhibition.**

19
20
21 Functional validation of novel potential cancer targets such as the protein methyltransferase
22
23 SMYD2 relies on appropriate model systems in vitro as well as in vivo. Additionally, chemical
24
25 probe inhibitors also suitable for in vivo applications are highly desirable. Most reported
26
27 activities of SMYD2 are not directly involved in survival signaling of cancer cells. Hence, in
28
29 vitro proliferation assays may not adequately cover the full phenotype of SMYD2 inhibition, and
30
31 more complex (*in vivo*) assays are thus required. The research work characterizing SMYD2 in
32
33 heart and skeletal muscle cells by knockdown experiments *in vivo*^{15,24,25} clearly illustrates the
34
35 complex underlying biology of SMYD2 and the necessity for chemical probes suitable for in
36
37 vivo applications. Therefore, we were interested in establishing if SMYD2 methylation activity
38
39 in tumor cells can be inhibited by (S)-4 in vivo. To this end, mice bearing subcutaneous tumor
40
41 xenografts (tumor tissue derived from the SMYD2-overexpressing KYSE-150 cell line) were
42
43 treated orally with 10, 30, 70 or 100 mg/kg (S)-4, or vehicle (PEG 400/water 8:2), once daily for
44
45 3 days. After the treatment period, tumors were harvested and analyzed ex vivo for methylation
46
47 of AHNK by dot-blotting. For detection of the methylation signals, SY46 methylation antibody
48
49 was used (see Figure 7A and Supplementary Figure S2A-F). (S)-4 significantly reduced the
50
51 methylation with doses starting from 30 mg/kg, with most significant effects in the 100 mg/kg
52
53
54
55
56
57
58
59
60

1
2
3 treated group ($P < 0.001$, Student's t test) (Figure 9A). Treatment with 10 mg/kg (S)-4 resulted in
4
5 no significant effect on the methylation level. Exposure at 10 mg/kg is close to the level of the
6
7 cellular IC_{50} for ~9 hours, which may indicate a need for an even higher exposure as the IC_{50} to
8
9 achieve in vivo effects on demethylation.
10
11

12
13
14 Then the KYSE-150 esophageal xenograft model was used to evaluate if the observed
15
16 improved apoptosis induction in the in vitro setting after treatment with doxorubicin (Figure 8B)
17
18 could translate to antitumor efficacy in vivo. Four groups of tumor-bearing mice were treated as
19
20 follows: Group 1 (control group) was only treated with vehicle (Solutol/ethanol/water 1:1:8) iv
21
22 q.d. and once at day 4 with the vehicle used for doxorubicin (saline) iv; Group 2 was treated with
23
24 (S)-4 at 500 mg/kg po q.d.; Group 3 was treated with 10 mg/kg doxorubicin iv once at day 4;
25
26 Group 4 was treated with a combination of (S)-4 and doxorubicin. There was a slight reduction
27
28 in area (Figure 9B) and weight (Figure 9C) of tumors from mice treated with the combination of
29
30 (S)-4 and doxorubicin relative to tumors from the control group. Combination treatment only
31
32 resulted in a minor increase in treatment-related body weight loss (Figure 9D). The combination
33
34 treatment reached a T/C level (based on tumor weight) of 0.46, which is significant (Figure 9C).
35
36 Therefore combination of a SMYD2 inhibitor with a chemotherapeutic agent resulted in reduced
37
38 cancer cell growth *in vivo*. In comparison, the monotherapy groups treated with only doxorubicin
39
40 or (S)-4 showed no significant antitumor efficacy relative to the vehicle control group. These
41
42 data are consistent with the observed limited cellular proliferation effects of (S)-4 in the cell line
43
44 panel (Figure 8A) and indicate that, in contrast to SMYD2 knockdown,² a catalytic inhibition
45
46 may be insufficient to induce cell death in the KYSE-150 esophageal model. Furthermore, the
47
48 monotherapeutic approach with doxorubicin did not result in any antitumor efficacy in the
49
50 KYSE-150 xenograft model.
51
52
53
54
55
56
57
58
59
60

CONCLUSION

In summary, we have identified (*S*)-**4** as a potent, selective and cell-active, substrate-competitive inhibitor of SMYD2. Our data show that SMYD2 inhibition can enhance efficacy of doxorubicin in vivo, which confirms our in vitro observation of higher caspase 3/7 activation (Figure 8B). Our results (*S*)-**4** are also in agreement with an earlier study¹³ where an increased apoptosis induction in cells with an SMYD2 knockdown was observed. Nonetheless, in our initial explorative in vivo study with (*S*)-**4**, effects on xenografted tumors were only moderate. In addition, high doses of (*S*)-**4** were needed in vitro as well as in vivo relative to the concentration needed to achieve effects on methylation. Therefore, we cannot exclude the possibility that additional, so-far unexplored activities of SMYD2 might be responsible for the observed effects. This again underlines the necessity to identify suitable chemical probes for more extensive target validation campaigns to fully explore the complex biology of SMYD2 and other targets. In this regard, (*S*)-**4** will be a highly valuable tool for the further exploration of SMYD2 biology, not only for in vitro but also for in vivo studies.

EXPERIMENTAL SECTION

Chemistry

General Procedures. All reagents and solvents were used as purchased, unless otherwise specified. All final products were at least 95% pure, as determined by analytical HPLC.

Materials. Intermediate **10a** and compounds **5**, **6** and **12–24** were synthesized according to the methods described previously.³⁷ ¹H NMR and determined to be >95%. ¹H NMR spectra were

recorded on Bruker Avance III HD spectrometers operating at 300, 400, or 500 MHz. The chemical shifts (δ) reported are given in parts per million (ppm), and the coupling constants (J) are in hertz (Hz). The spin multiplicities are reported as s = singlet, br s = broad singlet, d = doublet, t = triplet, q = quartet, m = multiplet, and br = broad. The LC/MS analysis was performed on Waters Acquity UPLCMS SingleQuad with a Acquity UPLC BEH C18 column (1.7 μ m, 50x2.1mm) at 60 °C, using water + 0.1 vol % formic acid (99%) and acetonitrile as mobile phase at a flow rate of 0.8 ml/min and a DAD detector (210-400 nm). LC/MS/MS was performed on a CTC PAL autosampler, an Agilent 1200 HPLC, and a ABSciex 4000 mass spectrometer.

Assignment of stereochemistry. For all separated enantiomers, it was assumed based on the co-crystal structure of **4**, that the active enantiomer (SMYD2 inhibition) has *S*-configuration.

Phenyl 4-[[Allyloxy]carbonyl]amino-3-(4-bromophenyl)-*N*-cyano-4,5-dihydro-1*H*-pyrazole-1-carboximidate (10b). Compound **10b** was prepared as described for **10d**. Starting from **7b** (37.7 g, 0.18 mol), **10b** was obtained as white solid (40.1 g, 49% over 4 steps). ¹H NMR (400 MHz, CDCl₃): δ = 4.26–4.42 (m, 3H), 4.66 (dd, J = 13.3, 6.0 Hz, 1H), 4.74 (dd, J = 13.1, 5.8 Hz, 1H), 5.30 (d, J = 10.3 Hz, 1H), 5.40 (d, J = 16.8 Hz, 1H), 5.67 (td, J = 8.8, 4.5 Hz, 1H), 6.00 (ddt, J = 16.8, 11.0, 5.6 Hz, 1H), 7.02–7.11 (m, 2H), 7.19–7.34 (m, 5H), 7.58 (d, J = 8.5 Hz, 2H). LC-MS (ESI): m/z = 468.1/470.1 [$M + H$]⁺.

Phenyl 4-[[Allyloxy]carbonyl]amino-3-(4-chloro-3,5-dimethylphenyl)-*N*-cyano-4,5-dihydro-1*H*-pyrazole-1-carboximidate (10c). Compound **10c** was prepared as described for **10d**. Starting from **7c** (35 g, 0.15 mol) to obtain **10c** (29.3 g, 43% over 4 steps) as white solid. ¹H NMR (400 MHz, [D]₆DMSO): δ = 2.32 (s, 6H), 4.03–4.18 (m, 1H), 4.39–4.61 (m, 2H), 5.06–

5.27 (m, 2H), 5.49–5.66 (m, 1H), 5.79–5.94 (m, 1H), 5.75–5.95 (m, 1H), 7.26 (d, $J = 7.8$ Hz, 2H), 7.30–7.37 (m, 1H), 7.41–7.55 (m, 2H), 7.56–7.73 (m, 2H), 8.17 (d, $J = 8.7$ Hz, 1H). LC-MS (ESI): $m/z = 452.2$ $[M + H]^+$.

Phenyl 4-{[(Allyloxy)carbonyl]amino}-*N*-cyano-3-(3,4-dichlorophenyl)-4,5-dihydro-1*H*-pyrazole-1-carboximidate (10d). To a stirred solution of 2-amino-1-(3,4-dichlorophenyl)ethanone hydrochloride (1:1) (**7d**; 116 g, 0.480 mol) in water (500 mL) was added allyl chloroformate (56.5 mL, 0.530 mol) in DCM (800 mL). The reaction mixture was cooled to 0 °C and K_2CO_3 (207 g, 1.49 mol) in water (1 L) was added dropwise over 1 h. The mixture was allowed to warm to rt, stirred overnight, then diluted with DCM (500 mL). The organic phase was washed with saturated aqueous NH_4Cl solution (400 mL) followed by brine (500 mL), then dried over $MgSO_4$, filtered and concentrated in vacuo. The crude mixture was purified by dry flash column chromatography (eluent: DCM/heptane 2:1, 3:1, 4:1; DCM; EtOAc) to yield allyl [2-(3,4-dichlorophenyl)-2-oxoethyl]carbamate (**8d**; 120 g, 87%) as a white crystalline solid. 1H NMR (400 MHz, $CDCl_3$): $\delta = 4.62$ (d, $J = 5.5$ Hz, 2H), 4.68 (d, $J = 4.6$ Hz, 2H), 5.25 (dd, $J = 1.4, 10.5$ Hz, 1H), 5.35 (dd, $J = 1.4, 16.9$ Hz, 1H), 5.72 (br s, 1H), 5.94 (m, 1H), 7.60 (d, $J = 8.2$ Hz, 1H), 7.79 (dd, $J = 2.1, 8.5$ Hz, 1H), 8.06 (d, $J = 1.8$ Hz, 1H). LC-MS (ESI): $m/z = 288.1$ $[M + H]^+$. To a stirred suspension of **8d** (50.0 g, 0.174 mol) in EtOH (390 mL) was added formaldehyde solution (20 mL, 0.261 mol; 37 wt% in water) followed by the dropwise addition of piperidine (26 mL, 0.261 mol) in EtOH (130 mL) over 30 min. The reaction mixture was stirred overnight; TLC indicated consumption of **8d**. The volatiles were removed by evaporation to yield an orange oil which was not further purified. To a solution of this crude material in EtOH (480 mL) was added hydrazine monohydrate (29.6 mL, 0.609 mol) and the reaction mixture was heated to reflux for 2.5 h. Then, the mixture was allowed to cool to rt,

concentrated and poured over ice-cooled saturated NH_4Cl solution (300 mL). The crude product was extracted with EtOAc (1.5 L) and the combined organic layers were washed with brine (300 mL), then dried over MgSO_4 , filtered and concentrated to yield allyl [3-(3,4-dichlorophenyl)-4,5-dihydro-1*H*-pyrazol-4-yl]carbamate (**9d**; 50.0 g, 91%) as a pale yellow solid. ^1H NMR (400 MHz, $[\text{D}]_6\text{DMSO}$): δ = 3.24 (m, 1H), 3.59 (m, 1H), 4.39–4.54 (m, 2H), 5.08–5.25 (m, 3H), 5.79–5.90 (m, 1H), 7.52 (dd, J = 1.8, 8.3 Hz, 1H), 7.57 (br s, 1H), 7.59 (m, 1H), 7.68 (d, J = 1.8 Hz, 1H), 7.84 (d, J = 8.7 Hz, 1H). LC-MS (ESI): m/z = 314.1 $[\text{M} + \text{H}]^+$. To a stirred suspension of **9d** (50.0 g, 0.159 mol) in *i*-PrOH (860 mL) was added diphenyl *N*-cyanocarbonimidate (38.0 g, 0.159 mol). The reaction mixture was heated to reflux, at which point the suspension dissolved into solution; after a further 10 min at reflux, a white precipitate formed. The mixture was stirred at reflux for a further 1 h, then allowed to slowly cool to rt overnight. The precipitate was collected by filtration and washed with Et_2O (2×250 mL). The resulting white solid was allowed to dry to yield **10d** (48.6 g, 67%) as a white solid. ^1H NMR (400 MHz, $[\text{D}]_6\text{DMSO}$): δ = 4.13 (apparent d, J = 8.2 Hz, 1H), 4.47 (m, 3H), 5.14 (m, 2H), 5.51–5.63 (m, 1H), 5.79–5.90 (m, 1H), 7.23 (d, J = 7.3 Hz, 2H), 7.30 (t, J = 7.8 Hz, 1H), 7.45 (m, 2H), 7.79 (br m, 2H), 7.97 (br s, 1H), 8.19 (d, J = 8.7 Hz, 1H). LC-MS (ESI): m/z = 458.0 $[\text{M} + \text{H}]^+$.

Phenyl 4-[(Allyloxy)carbonyl]amino}-3-(4-chloro-3-methylphenyl)-*N*-cyano-4,5-dihydro-1*H*-pyrazole-1-carboximidate (10e**).** Compound **10e** was prepared as described for **10d**. Starting from **7e** (3.1 g, 13.9 mmol) to obtain **10e** (2.12 g, 34.4% over 4 steps) as white solid. ^1H NMR (400 MHz, CDCl_3): δ = 2.18 (s, 3H), 4.30 (d, J = 6.4 Hz, 2H), 4.64 (d, J = 6.0 Hz, 2H), 5.24 (d, J = 10.5 Hz, 1H), 5.34 (d, J = 16.9 Hz, 1H), 5.60–5.70 (m, 1H), 5.94 (ddt, J = 5.6, 10.9,

16.8 Hz, 1H), 6.89–7.35 (m, 7H), 7.48 (m, 1H), 7.54 (m, 1H). LC-MS (ESI): m/z = 438.2 [$M + H$]⁺.

Phenyl 4-[[{(Allyloxy)carbonyl]amino}-3-(1,3-benzodioxol-5-yl)-*N*-cyano-4,5-dihydro-1*H*-pyrazole-1-carboximidate (10f). Compound **10f** was prepared as described for **10d**, starting from **7f** (12.0 g, 55.7 mmol) to obtain **10f** (9.1 g, 38% over 4 steps) as white solid. ¹H NMR (400 MHz, [D]₆DMSO): δ = 4.05–4.08 (m, 1H), 4.43–4.47 (m, 3H), 5.1–5.2 (m, 2H), 5.50–5.55 (m, 1H), 5.80–5.90 (m, 1H), 6.08 (s, 2H), 7.05 (d, J = 7.8 Hz, 1H), 7.21–7.27 (m, 2H), 7.27–7.41 (m, 3H), 7.43–7.50 (m, 2H), 8.16 (d, J = 8.7 Hz, 1H). LC-MS (ESI): m/z = 434.2 [$M + H$]⁺.

General Procedure for the Synthesis of Allyl [1-(*N'*-Cyano-*N*-arylcarbamimidoyl)-3-phenyl-4,5-dihydro-1*H*-pyrazol-4-yl]carbamates 11j–s. To a stirred solution of the respective aniline derivative (3 equiv) in anhydrous THF (2 mL/mmol) at –78 °C was added *n*-BuLi (3 equiv, 2 M in hexane) dropwise, while maintaining the reaction temperature below –65 °C. The reaction mixture was stirred at –78 °C for 1 h, then the respective phenyl 4-[[{(allyloxy)carbonyl]amino}-*N*-cyano-3-phenyl-4,5-dihydro-1*H*-pyrazole-1-carboximidate **10** (1 equiv) in anhydrous THF (30 mL/mmol) was added dropwise, while maintaining the reaction temperature below –65 °C. The reaction mixture was stirred at –78 °C for 2 h, then slowly poured over saturated NH₄Cl solution (30 mL/mmol based on **10**). The crude product was extracted into EtOAc (30 mL/mmol); the combined organic layers were washed with brine (15 mL/mmol), dried over MgSO₄, filtered and concentrated. The crude solid was precipitated from a minimum volume of EtOAc, collected by filtration and washed with Et₂O to give the corresponding intermediate **11**.

Allyl [3-(4-Bromophenyl)-1-{*N'*-cyano-*N*-[3-(difluoromethoxy)phenyl]carbamimidoyl}-4,5-dihydro-1*H*-pyrazol-4-yl]carbamate (11j). Compound **11j** was prepared from **10b** (5.0 g, 10.7 mmol) and 3-(difluoromethoxy)aniline. **11j** was not pure after chromatography, and was used as such in further steps (3.8 g, purity 77 %-UV, 51 %). LC-MS (ESI): $m/z = 533.1$ $[M + H]^+$.

Allyl [3-(4-Chloro-3,5-dimethylphenyl)-1-{*N'*-cyano-*N*-[3-(difluoromethoxy)phenyl]carbamimidoyl}-4,5-dihydro-1*H*-pyrazol-4-yl]carbamate (11k). Compound **11k** was prepared from **10c** (10.0 g, 22.1 mmol) and 3-(difluoromethoxy)aniline. **11k** was obtained as white solid (9.1 g, 80 %). ^1H NMR (400 MHz, CDCl_3): $\delta = 2.32$ (s, 6H), 4.3–4.6 (m, 4H), 5.13 (dd, $J = 1.1$, 10.3 Hz, 1H), 5.19 (dd, $J = 1.4$, 17.4 Hz, 1H), 5.5–5.6 (m, 1H), 5.7–5.9 (m, 1H), 6.53 (t, $J = 73.8$ Hz, 1H), 6.87 (br d, $J = 8.7$ Hz, 1H), 7.1–7.3 (m, 4H), 7.50 (s, 2H), 8.35 (s, 1H). LC-MS (ESI): $m/z = 517.2$ $[M + H]^+$.

Allyl [1-{*N'*-Cyano-*N*-[3-(difluoromethoxy)phenyl]carbamimidoyl}-3-(3,4-dichlorophenyl)-4,5-dihydro-1*H*-pyrazol-4-yl]carbamate (11l). Compound **11l** was prepared from **10d** (20.0 g, 43.6 mmol) and 3-(difluoromethoxy)aniline. **11l** was obtained as white solid (21.2 g, 93 %). ^1H NMR (400 MHz, $[\text{D}]_6\text{DMSO}$): $\delta = 4.08$ (dd, $J = 4.6$, 11.9 Hz, 1H), 4.36–4.53 (m, 3H), 5.11 (dd, $J = 1.4$, 10.5 Hz, 1H), 5.17 (dd, $J = 1.4$, 17.4 Hz, 1H), 5.50–5.59 (m, 1H), 5.77–5.90 (m, 1H), 6.99 (dd, $J = 2.3$, 8.2 Hz, 1H), 7.16 (m, 1H), 7.21 (t, $J = 73.7$ Hz, 1H), 7.22 (m, 1H), 7.39 (t, $J = 8.3$ Hz, 1H), 7.73–7.81 (m, 2H), 8.15 (d, $J = 1.4$ Hz, 1H), 8.17 (d, $J = 8.7$ Hz, 1H), 9.79 (br s, 1H). LC-MS (ESI): $m/z = 523.2$ $[M + H]^+$.

Allyl [3-(4-Chloro-3-methylphenyl)-1-{*N'*-cyano-*N*-[3-(difluoromethoxy)phenyl]carbamimidoyl}-4,5-dihydro-1*H*-pyrazol-4-yl]carbamate (11m). Compound **11m** was prepared from **10e** (10.0 g, 22.8 mmol) and 3-(difluoromethoxy)aniline. **11m** was obtained as

white solid (9.6 g, 84 %). ^1H NMR (400 MHz, $[\text{D}]_6\text{DMSO}$): δ = 2.33–2.40 (m, 3H), 4.03–4.15 (m, 1H), 4.41–4.56 (m, 3H), 5.13–5.36 (m, 2H), 5.53–5.63 (m, 1H), 5.82–5.94 (m, 1H), 7.00–7.08 (m, 1H), 7.19–7.29 (m, 2H), 7.25 (t, J = 74 Hz, 1H, partially masked by other peaks), 7.40–7.49 (m, 1H), 7.55 (d, J = 8.4 Hz, 1H), 7.73 (dd, J = 1.7, 8.2 Hz, 1H), 7.84–7.90 (m, 1H), 8.2 (br d, J = 8.6 Hz, 1H), 9.75 (br s, 1H). LC-MS (ESI): m/z = 503.2 $[\text{M} + \text{H}]^+$.

Allyl [3-(1,3-Benzodioxol-5-yl)-1-{ N' -cyano- N -[3-(difluoromethoxy)phenyl]-carbamimidoyl}-4,5-dihydro-1*H*-pyrazol-4-yl]carbamate (11n). Compound **11n** was prepared from **10f** (2.0 g, 4.6 mmol) and 3-(difluoromethoxy)aniline. **11n** was obtained as white solid (1.7 g, 74 %). ^1H NMR (400 MHz, $[\text{D}]_6\text{DMSO}$): δ = 4.09 (dd, J = 4.6, 11.9 Hz, 1H), 4.43 (t, J = 11.2 Hz, 1H), 4.50 (d, J = 4.1 Hz, 2H), 5.16 (dd, J = 1.4, 10.5 Hz, 1H), 5.22 (dd, J = 1.6, 17.2 Hz, 1H), 5.49–5.60 (m, 1H), 5.82–5.93 (m, 1H), 6.11 (s, 2H), 6.95–7.09 (m, 2H), 7.16–7.32 (m, 4H), 7.39 (m, 1H), 7.61 (d, J = 1.4 Hz, 1H), 8.21 (d, J = 8.7 Hz, 1H), 9.63 (s, 1H). LC-MS (ESI): m/z = 499.2 $[\text{M} + \text{H}]^+$.

Allyl [1-{ N' -Cyano- N -[3-(trifluoromethoxy)phenyl]carbamimidoyl}-3-(3,4-dichlorophenyl)-4,5-dihydro-1*H*-pyrazol-4-yl]carbamate (11o). Compound **11o** was prepared from **10d** (10 g, 21.8 mmol) and 3-(trifluoromethoxy)aniline. **11o** was obtained as beige solid (7.4 g, 63 %). ^1H NMR (400 MHz, $[\text{D}]_6\text{DMSO}$): δ = 4.13 (dd, J = 4.8, 11.9 Hz, 1H), 4.42–4.56 (m, 3H), 5.12–5.25 (m, 2H), 5.50–5.63 (m, 1H), 5.83–5.94 (m, 1H), 7.19 (br d, J = 8.1 Hz, 1H), 7.35–7.44 (m, 2H), 7.46–7.56 (m, 1H), 7.77–7.85 (m, 2H), 8.13–8.24 (m, 2H), 9.89 (br s, 1H). LC-MS (ESI): m/z = 540.8 $[\text{M} + \text{H}]^+$.

Allyl {1-[N' -Cyano- N -(3-methoxyphenyl)carbamimidoyl]-3-(3,4-dichlorophenyl)-4,5-dihydro-1*H*-pyrazol-4-yl]carbamate (11p). Compound **11p** was prepared from **10d** (2.0 g, 4.4

mmol) and 3-methoxyaniline. **11p** was obtained as white solid (1.5 g, 71 %). ¹H NMR (400 MHz, [D]₆DMSO): δ = 3.3 (s, 3H, masked by water signal), 3.97–4.07 (m, 1H), 4.33–4.48 (m, 1H), 5.40 (s, 1H), 5.74–5.82 (m, 1H), 6.95 (br d, *J* = 7.1 Hz, 1H), 7.14–7.26 (m, 3H), 7.34–7.43 (m, 1H), 7.73 (d, *J* = 8.5 Hz, 1H), 7.81 (dd, *J* = 1.9, 8.5 Hz, 1H), 8.08 (s, 1H), 8.76 (br d, *J* = 8.8 Hz, 1H), 9.51 (br s, 1H). LC-MS (ESI): *m/z* = 487.1 [M + H]⁺.

Allyl [1-{*N'*-Cyano-*N*-[6-(difluoromethoxy)pyridin-2-yl]carbamimidoyl}-3-(3,4-dichlorophenyl)-4,5-dihydro-1*H*-pyrazol-4-yl]carbamate (**11q**). Compound **11q** was prepared from **10d** (5.0 g, 10.9 mmol) and 6-(difluoromethoxy)pyridin-2-amine. **11q** was obtained as off-white solid (2.9 g, 43 %). ¹H NMR (400 MHz, [D]₆DMSO): δ = 3.95 (dd, *J* = 5.0, 12.4 Hz, 1H), 4.32 (t, *J* = 11.7 Hz, 1H), 4.4–4.5 (m, 2H), 5.13 (m, 2H), 5.51 (m, 1H), 5.84 (m, 1H), 6.82 (d, *J* = 8.2 Hz, 1H), 7.13 (d, *J* = 7.8 Hz, 1H), 7.58 (t, *J* = 72.8 Hz, 1H), 7.7–7.8 (m, 2H), 7.91 (t, *J* = 7.8 Hz, 1H), 8.05 (d, 1H), 8.18 (d, *J* = 1.8 Hz, 1H), 10.45 (s, 1H). LC-MS (ESI): *m/z* = 524.1 [M + H]⁺.

Allyl [1-{*N*-[4-Chloro-3-(difluoromethoxy)phenyl]-*N'*-cyanocarbamidoyl}-3-(3,4-dichlorophenyl)-4,5-dihydro-1*H*-pyrazol-4-yl]carbamate (**11r**). Compound **11r** was prepared from **10d** (2.0 g, 4.4 mmol) and 4-chloro-3-(difluoromethoxy)aniline. **11r** was obtained as white solid (1.5 g, 62 %). ¹H NMR (400 MHz, [D]₆DMSO): δ = 4.01–4.17 (m, 1H), 4.42–4.56 (m, 3H), 5.12–5.25 (m, 2H), 5.53–5.64 (m, 1H), 5.82–5.94 (m, 1H), 7.28 (t, *J* = 73 Hz, 1H, partially masked by other peaks), 7.34 (dd, *J* = 2.4, 8.7 Hz, 1H), 7.42 (m, 1H), 7.61 (d, *J* = 8.6 Hz, 1H), 7.81 (s, 2H), 8.13–8.25 (m, 2H), 9.91 (br s, 1H). LC-MS (ESI): *m/z* = 557.1 [M + H]⁺.

Allyl [1-{*N'*-Cyano-*N*-[3-(difluoromethoxy)-5-fluorophenyl]carbamimidoyl}-3-(3,4-dichlorophenyl)-4,5-dihydro-1*H*-pyrazol-4-yl]carbamate (**11s**). Compound **11s** was prepared

from **10d** (1.6 g, 3.4 mmol) and 3-(difluoromethoxy)-5-fluoroaniline. **11s** was obtained as white solid (0.8 g, 45 %). ^1H NMR (400 MHz, $[\text{D}]_6\text{DMSO}$): δ = 4.13 (dd, J = 4.6, 11.9 Hz, 1H), 4.41–4.53 (m, 3H), 5.10–5.25 (m, 2H), 5.51–5.63 (m, 1H), 5.78–5.94 (m, 1H), 6.96 (dd, J = 2.2, 9.7 Hz, 1H), 7.10 (d, J = 5.1 Hz, 1H), 7.18 (br d, J = 10.9 Hz, 1H), 7.29 (t, J = 73 Hz, 1H, partially masked by other peaks), 7.74–7.85 (m, 2H), 8.10–8.30 (m, 2H), 9.88 (br s, 1H). LC-MS (ESI): m/z = 541.2 $[\text{M} + \text{H}]^+$.

***N*-(1-{*N'*-Cyano-*N*-[3-(difluoromethoxy)phenyl]carbamimidoyl}-3-phenyl-4,5-dihydro-1*H*-pyrazol-4-yl)-*N*-ethyl-2-hydroxyacetamide (25) and *N*-[3-(4-Bromophenyl)-1-{*N'*-cyano-*N*-[3-(difluoromethoxy)phenyl]carbamimidoyl}-4,5-dihydro-1*H*-pyrazol-4-yl]-*N*-ethyl-2-hydroxyacetamide (26).** To a stirred solution of **11j** (3.8 g, 77 %-UV, 5.5 mmol) in degassed THF (150 mL) was added 1,3-dimethylbarbituric acid (1.8 g, 11.0 mmol), followed by tetrakis(triphenylphosphine)palladium(0) $[\text{Pd}(\text{PPh}_3)_4]$; 0.25 g, 0.22 mmol]. The reaction mixture was stirred under argon for 12 h, then cautiously quenched with saturated NaHCO_3 solution (150 mL) and extracted into EtOAc (150 mL). The organic layer was washed with brine (100 mL), then dried over Na_2SO_4 , filtered and concentrated. The crude material was purified by dry flash column chromatography (eluent: EtOAc; MeOH) to yield 4-amino-3-(4-bromophenyl)-*N'*-cyano-*N*-[3-(difluoromethoxy)phenyl]-4,5-dihydro-1*H*-pyrazole-1-carboximidamide (2.4 g, 95 %-UV, 92%). ^1H NMR (400 MHz, $[\text{D}]_6\text{DMSO}$): δ = 2.38 (br s, 2H), 4.02 (dd, J = 4.4, 11.5 Hz, 1H), 4.37 (dd, J = 9.9, 11.4 Hz, 1H), 4.81 (dd, J = 4.5, 9.9 Hz, 1H), 6.98 (dd, J = 2.0, 8.1 Hz, 1H), 7.22 (t, J = 74.0 Hz, 1H), 7.20–7.23 (m, 1H), 7.27 (ddd, J = 0.8, 2.0, 8.1 Hz, 1H), 7.40 (t, J = 8.1 Hz, 1H), 7.64–7.70 (m, 2H), 7.98–8.03 (m, 2H), 9.62 (br s, 1H). LC-MS (ESI): m/z = 449.3 $[\text{M} + \text{H}]^+$. To the amine product (2.30 g, 5.1 mmol) in MeOH (70 mL) at rt was added acetaldehyde (0.27 g, 6.1 mmol). The reaction mixture was stirred at rt for 1 h, and at 40 °C for 1

h, then it was cooled to 0 °C and NaBH₄ (0.22 g, 5.7 mmol) was added in small portions. The mixture was stirred at rt for 1 h, then poured over saturated NaHCO₃ solution (10 mL). The volatiles were removed by evaporation and the resulting aqueous slurry was extracted with EtOAc (2 × 10 mL). The combined organic layers were washed with brine (100 mL), then dried over Na₂SO₄, filtered and concentrated to yield a crude black oil. The crude material was purified by dry flash column chromatography (eluent: DCM; MeOH) to yield 3-(4-bromophenyl)-*N'*-cyano-*N*-[3-(difluoromethoxy)phenyl]-4-(ethylamino)-4,5-dihydro-1*H*-pyrazole-1-carboximidamide (1.11 g, 45%) as the main *N*-ethylation product. LC-MS (ESI): *m/z* = 477.1 [M + H]⁺. The corresponding debrominated derivative *N'*-cyano-*N*-[3-(difluoromethoxy)phenyl]-4-(ethylamino)-3-phenyl-4,5-dihydro-1*H*-pyrazole-1-carboximidamide (0.41 g, 19%) was obtained as a byproduct. LC-MS (ESI): *m/z* = 398.3 [M + H]⁺. To the debrominated byproduct (410 mg, 1 mmol) in DCM (15 mL) were added Et₃N (0.15 mL, 1.1 mmol), acetoxyacetyl chloride (0.12 mL, 1.1 mmol) and DMAP (126 mg, 1 mmol) and the mixture was stirred at rt for 1 h. EtOAc (15 mL) was added, and the mixture was washed with saturated aqueous NH₄Cl solution (20 mL) and brine (20 mL). The organic phase was dried over Na₂SO₄ and concentrated. The crude product was purified by dry flash column chromatography (eluent: DCM; MeOH) to yield 504 mg of an impure intermediate, which was dissolved in MeOH (12 mL), K₂CO₃ (140 mg, 1.01 mmol) was added, and the mixture was heated to reflux for 30 min. After cooling, to the reaction mixture was added saturated aqueous NH₄Cl, and the mixture was extracted with EtOAc. The organic phase was dried over Na₂SO₄, concentrated and the residue was purified by flash column chromatography (eluent: DCM, MeOH) and subsequent preparative HPLC to yield *N*-(1-{*N'*-cyano-*N*-[3-(difluoromethoxy)phenyl]carbamiimidoyl}-3-phenyl-4,5-dihydro-1*H*-pyrazol-4-yl)-*N*-ethyl-2-

hydroxyacetamide (**25**; 50 mg, 10%). ¹H NMR (300 MHz, [D]₆DMSO): δ = 1.03 (br s, 3H), 3.16–3.33 (m, 2H), 3.92–4.25 (m, 3H), 4.47 (br t, *J* = 11.7 Hz, 1H), 4.75 (br t, *J* = 5.5 Hz, 1H), 6.94–7.03 (m, 1H), 7.19–7.30 (m, 3H), 7.36–7.52 (m, 4H), 7.75–7.84 (m, 2H), 9.77 (br s, 1H). LC-MS (ESI): *m/z* = 457.2 [M + H]⁺.

To the main product from the N-ethylation step (1.1 g, 2.3 mmol) in DCM (30 mL) were added Et₃N (0.34 mL, 2.4 mmol), acetoxyacetyl chloride (0.27 mL, 2.4 mmol) and DMAP (282 mg, 2.3 mmol) and the mixture was stirred at rt for 1 h. EtOAc (30 mL) was added, and the mixture was washed with saturated aqueous NH₄Cl solution (40 mL) and brine (40 mL). The organic phase was dried over Na₂SO₄ and concentrated. The crude product was purified by dry flash column chromatography (eluent: DCM; MeOH) to yield 1.2 g of an impure intermediate. 200 mg of this intermediate were dissolved in MeOH (5 mL), K₂CO₃ (48 mg, 0.35 mmol) was added, and the mixture was heated to reflux for 30 min. After cooling, the reaction mixture was concentrated and the residue was purified by HPLC to yield (*N*-[3-(4-bromophenyl)-1-{*N'*-cyano-*N*-[3-(difluoromethoxy)phenyl]carbamimidoyl}-4,5-dihydro-1*H*-pyrazol-4-yl]-*N*-ethyl-2-hydroxyacetamide (**26**; 50 mg, 24%). ¹H NMR (400 MHz, [D]₆DMSO): δ = 1.05 (br s, 3H), 3.27–3.36 (m, 2H), 3.98–4.18 (m, 3H), 4.48 (t, *J* = 11.7 Hz, 1H), 4.72 (t, *J* = 4.9 Hz, 1H), 7.00 (d, *J* = 7.8 Hz, 1H), 7.21 (s, 1H), 7.23 (t, *J* = 74.0 Hz, 1H), 7.26 (d, *J* = 8.3 Hz, 1H), 7.41 (t, *J* = 8.2 Hz, 1H), 7.67 (d, *J* = 8.5 Hz, 2H), 7.73 (d, *J* = 8.3 Hz, 2H), 9.78 (br s, 1H). LC-MS (ESI): *m/z* = 535.1 [M + H]⁺.

***N*-[3-(4-Chloro-3,5-dimethylphenyl)-1-{*N'*-cyano-*N*-[3-(difluoromethoxy)phenyl]-carbamimidoyl}-4,5-dihydro-1*H*-pyrazol-4-yl]-*N*-ethyl-2-hydroxyacetamide (**27**).**

Compound **27** was prepared as described for **4**, starting from **11k** (4.9 g, 9.6 mmol). **27** was obtained as grey solid (1.6 g, 32 % over 3 steps). ¹H NMR (300 MHz, [D]₆DMSO): δ = 1.05 (br

s, 3H), 2.32 (s, 6H), 3.23–3.44 (m, 2H), 3.94–4.15 (m, 3H), 4.44 (br t, $J = 11.7$ Hz, 1H), 4.69 (br s, 1H), 6.92–7.02 (m, 1H), 7.14–7.27 (m, 2H), 7.33–7.43 (m, 1H), 7.56 (s, 2H), 9.73 (br s, 1H). LC-MS (ESI): $m/z = 518$ $[M + H]^+$.

***N*-[1- $\{N'$ -Cyano-*N*-[3-(difluoromethoxy)phenyl]carbamimidoyl]-3-(3,4-dichlorophenyl)-4,5-dihydro-1*H*-pyrazol-4-yl]-*N*-ethyl-2-hydroxyacetamide (4).** To a stirred solution of **111** (14.2 g, 27.0 mmol) in degassed THF (370 mL) was added 1,3-dimethylbarbituric acid (17.0 g, 108 mmol), followed by $\text{Pd}(\text{PPh}_3)_4$ (2.40 g, 2.16 mmol). The reaction mixture was stirred under argon for 15 min, then cautiously quenched with saturated NaHCO_3 solution (400 mL) and extracted into EtOAc (400 mL). The organic layer was washed with brine (200 mL), then dried over MgSO_4 , filtered and concentrated. The crude material was purified by dry flash column chromatography (eluent: EtOAc/heptane 1:1, 2:1; EtOAc; MeOH/EtOAc 1:100) to yield 4-amino-*N'*-cyano-3-(3,4-dichlorophenyl)-*N*-[3-(difluoromethoxy)phenyl]-4,5-dihydro-1*H*-pyrazole-1-carboximidamide (9.3 g, 78%) as an orange oil. ^1H NMR (400 MHz, $[\text{D}]_6\text{DMSO}$): $\delta = 3.95\text{--}4.02$ (m, 1H, under EtOAc signal), 4.35 (m, 1H), 4.83 (dd, $J = 4.6, 9.6$ Hz, 1H), 7.01 (dd, $J = 2.1, 8.0$ Hz, 1H), 7.22 (t, $J = 2.1$ Hz, 1H), 7.24 (t, $J = 73.7$ Hz, 1H), 7.27 (m, 1H), 7.38 (t, $J = 7.8$ Hz, 1H), 7.48–7.61 (m, 1H), 7.72 (d, $J = 8.2$ Hz, 1H), 8.00 (dd, $J = 2.1, 8.5$ Hz, 1H), 8.31 (d, $J = 1.8$ Hz, 1H), 9.67 (br s, 1H). LC-MS (ESI): $m/z = 439.1$ $[M + H]^+$. To a stirred solution of the amine product (9.30 g, 21.2 mmol) in MeOH (170 mL) at 0 °C was added acetaldehyde (1.12 g, 25.4 mmol), followed by the portionwise addition of NaBH_4 (0.96 g, 25.4 mmol) over 20 min. The mixture was stirred for 30 min, then poured over saturated NaHCO_3 solution (100 mL). The volatiles were removed by evaporation and the resulting aqueous slurry was extracted with EtOAc (2×100 mL). The combined organic layers were washed with brine (100 mL), then dried over MgSO_4 , filtered and concentrated to yield a crude black oil. The crude material was purified

by dry flash column chromatography (eluent: EtOAc/heptane 1:1, EtOAc) to give a black oil, which was triturated with Et₂O to yield *N*'-cyano-3-(3,4-dichlorophenyl)-*N*-[3-(difluoromethoxy)phenyl]-4-(ethylamino)-4,5-dihydro-1*H*-pyrazole-1-carboximidamide (7.40 g, 75%) as a gray solid. ¹H NMR (400 MHz, [D]₆DMSO): δ = 0.98 (t, *J* = 6.6 Hz, 3H), 2.40–2.64 (m, 2H, partially under DMSO signal), 4.16–4.27 (m, 2H), 4.83 (m, 1H), 6.98 (dd, *J* = 2.3, 8.2 Hz, 1H), 7.21 (t, *J* = 2.1 Hz, 1H), 7.25 (t, *J* = 73.7 Hz, 1H), 7.27 (dt, *J* = 1.0, 8.1 Hz, 1H), 7.42 (t, *J* = 8.2 Hz, 1H), 7.76 (d, *J* = 8.7 Hz, 1H), 8.01 (dd, *J* = 2.1, 8.5 Hz, 1H), 8.33 (d, *J* = 1.8 Hz, 1H), 9.71 (br s, 1H). LC-MS (ESI): *m/z* = 467.2 [*M* + *H*]⁺. To this product (7.24 g, 15.5 mmol) in DCM (62 mL) was added saturated aqueous NaHCO₃ solution (72 mL). The biphasic mixture was stirred vigorously and cooled to 5 °C; acetoxyacetyl chloride (2.50 mL, 23.2 mmol) in DCM (10 mL) was added dropwise over 15 min. The mixture was stirred at 5 °C for 10 min, after which time LC analysis indicated total consumption of the starting material and only one major peak. The volatiles were removed by evaporation to yield an oily aqueous suspension to which K₂CO₃ (4.28 g, 31.0 mmol) was added, followed by MeOH (110 mL). The mixture was brought to reflux for 5 min then allowed to cool to rt, whereupon the product precipitated as a white solid. The solid was collected by filtration, washed with water (50 mL) and Et₂O (50 mL), and dried in vacuo to yield **4** (7.58 g, 93%) as a white powder. ¹H NMR (400 MHz, [D]₆DMSO): δ = 0.98–1.10 (m, 3H), 3.17–3.42 (m, 2H, partially under water signal), 3.94–4.17 (m, 3H), 4.46 (t, *J* = 11.7 Hz, 1H), 4.75 (t, *J* = 5.7 Hz, 1H), 6.98 (dd, *J* = 7.8, 1.8 Hz, 1H), 7.18 (br t, 1H), 7.22 (m, 1H), 7.23 (t, *J* = 8.2 Hz, 1H), 7.40 (t, 1H), 7.62 (dd, *J* = 8.2, 1.8 Hz, 1H), 7.7 (d, *J* = 8.2 Hz, 1H), 8.11 (d, *J* = 1.4 Hz, 1H), 9.85 (br s, 1H). LC-MS (ESI): *m/z* = 525.0 [*M* + *H*]⁺.

Compound **4** was separated into its enantiomers by chiral SFC (instrument: Sepiatec Prep SFC 100, column: Chiralpak ID 5 μm, 250 × 20 mm, eluent: CO₂/*i*-PrOH 7:3, flow: 80 mL/min,

temperature: 40 °C): t_R (min) = 3.35–4.40 [(*S*)-**4**], 7.31–9.00 [(*R*)-**4**]. Enantiomer (*S*)-**4**: SFC (Chiralpak ID 5 μ m, 100 \times 4.6 mm, CO₂/*i*-PrOH 7:3, flow: 4 mL/min, temperature: 37.5 °C): t_R (min) = 2.41. $[\alpha]_D -102$ (*c* 0.44, MeOH). Enantiomer (*R*)-**4**: SFC (Chiralpak ID 5 μ m, 100 \times 4.6 mm, CO₂/*i*-PrOH 7:3, flow: 4 mL/min, temperature: 37.5 °C): t_R (min) = 5.66. $[\alpha]_D +96$ (*c* 0.25, MeOH).

***N*-[3-(4-Chloro-3-methylphenyl)-1-{*N'*-cyano-*N*-[3-(difluoromethoxy)phenyl]carbamimidoyl}-4,5-dihydro-1*H*-pyrazol-4-yl]-*N*-ethyl-2-hydroxyacetamide (**28**).** Compound **28** was prepared as described for **4**, starting from **11m** (3.4 g, 6.6 mmol). **28** was obtained as yellow solid (537 mg, 16 % over 3 steps) ¹H NMR (500 MHz, [D]₂DCM): δ = 1.11 (br t, *J* = 6.8 Hz, 3H), 2.43 (s, 3H), 3.11–3.34 (m, 3H), 4.11–4.27 (m, 2H), 4.43–4.54 (m, 2H), 6.65 (t, *J* = 74.1 Hz, 1H), 7.00–7.08 (m, 1H), 7.32 (d, *J* = 7.3 Hz, 2H), 7.40–7.46 (m, 2H), 7.49 (dd, *J* = 10.1, 8.2 Hz, 1H), 7.72 (d, *J* = 1.3 Hz, 1H), 8.27 (s, 1H). LC-MS (ESI): *m/z* = 505.0 [M + H]⁺.

Compound **28** was separated into its enantiomers by chiral HPLC (instrument: Agilent Prep 1200, column: Chiralpak ID 5 μ m, 250 \times 30 mm, eluent: hexane/EtOH 7:3, flow: 50 mL/min): t_R (min) = 7.2–9.0 [(*R*)-**28**], 10.9–12.9 [(*S*)-**28**]. Enantiomer (*S*)-**28**: HPLC (Chiralpak ID 3 μ m, 100 \times 4.6 mm, hexane/EtOH 7:3, 1.0 mL/min): t_R (min) = 6.22. $[\alpha]_D -96.8$ (*c* 0.88, MeOH).

***N*-[3-(1,3-Benzodioxol-5-yl)-1-{*N'*-cyano-*N*-[3-(difluoromethoxy)phenyl]carbamimidoyl}-4,5-dihydro-1*H*-pyrazol-4-yl]-*N*-ethyl-2-hydroxyacetamide (**29**).** Compound **29** was prepared as described for **4**, starting from **11n** (870 mg, 2.0 mmol). **29** was obtained as off-white solid (432 mg, 43 % over 3 steps) ¹H NMR (400 MHz, [D]₆DMSO): δ = 0.99 (br s, 3H), 3.08–3.31 (m, 2H), 3.94–4.18 (m, 3H), 4.41 (br t, *J* = 11.2 Hz, 1H), 4.75 (br s, 1H), 6.07 (br d, *J* = 2.3 Hz,

2H), 6.96 (br d, $J = 8.2$ Hz, 2H), 7.11–7.27 (m, 4H), 7.35–7.43 (m, 1H), 7.48–7.63 (m, 2H), 9.68 (br s, 1H). LC-MS (ESI): $m/z = 501.2$ $[M + H]^+$.

***N*-[1- $\{N'$ -Cyano-*N*-[3-(trifluoromethoxy)phenyl]carbamimidoyl]-3-(3,4-dichlorophenyl)-4,5-dihydro-1*H*-pyrazol-4-yl]-*N*-ethyl-2-hydroxyacetamide (**30**).** Compound **30** was prepared as described for compound **4**, starting from **11o** (385 mg, 0.71 mmol). **30** was obtained as white solid (244 mg, 66 % over 3 steps). ^1H NMR (400 MHz, $[\text{D}]_6\text{DMSO}$): $\delta = 1.03$ (t, $J = 6.6$ Hz, 3H), 3.3–3.5 (m, 2H), 3.9–4.1 (m, 3H), 4.4–4.5 (m, 1H), 4.7–4.8 (m, 1H), 7.15 (d, 1H), 7.3–7.8 (m, 6H), 8.09 (s, 1H), 9.88 (s, 1H). LC-MS (ESI): $m/z = 542.9$ $[M + H]^+$.

Compound **30** was separated into its enantiomers by chiral SFC (instrument: Sepiatec: Prep SFC100, column: Chiralpak IE $5\mu\text{m}$ 250x20 mm, eluent: CO_2 /2-propanol 67/33, flow: 80 mL/min, temperature: 40 $^\circ\text{C}$): t_R (min) = 4.8–5.9 [(*R*)-**30**], 8.6–10.3 [(*S*)-**30**]. Enantiomer (*S*)-**30**: SFC (Chiralpak IE $5\mu\text{m}$ 100x4.6 mm, CO_2 /2-propanol 67/33, flow: 4.0 mL/min, temperature: 37.5 $^\circ\text{C}$): t_R (min) = 5.24. $[\alpha]_D -79$ (c 0.83, MeOH).

***N*-{1-[N' -Cyano-*N*-(3-methoxyphenyl)carbamimidoyl]-3-(3,4-dichlorophenyl)-4,5-dihydro-1*H*-pyrazol-4-yl]-*N*-ethyl-2-hydroxyacetamide (**31**).** Compound **31** was prepared as described for **4**, starting from **11p** (1.5 g, 3.1 mmol). **31** was obtained as yellow solid (325 mg, 21 % over 3 steps). ^1H NMR (400 MHz, $[\text{D}]_6\text{DMSO}$): $\delta = 1.04$ (br s, 3H), 3.14–3.27 (m, 1H), 3.74 (s, 3H), 3.99–4.14 (m, 3H), 4.38 (br t, $J = 11.9$ Hz, 1H), 4.72 (br t, $J = 5.6$ Hz, 1H), 5.85 (br s, 1H), 6.84 (m, 3H), 7.20 (br t, $J = 8.5$ Hz, 1H), 7.51–7.64 (m, 2H), 7.69–7.73 (m, 1H), 8.07 (br s, 1H), 9.75 (br s, 1H). LC-MS (ESI): $m/z = 489.2$ $[M + H]^+$.

Compound **31** was separated into its enantiomers by chiral HPLC (instrument: Agilent Prep 1200, column: Chiralpak IC $5\mu\text{m}$, 250×20 mm, eluent: MeOH/EtOH/ Et_2NH 50:50:0.1, flow:

20 mL/min, temperature: 23 °C): *t*R (min) = 5.0–6.0 [(*S*)-**31**], 6.75–8.0 [(*R*)-**31**]. Enantiomer (*S*)-**31**: HPLC (Chiralpak IC 5 μm, 150 × 4.6 mm, MeOH/EtOH/Et₂NH 50:50:0.1, 1.0 mL/min): *t*R (min) = 2.65. [α]_D –88.1 (*c* 1.0, MeOH).

N-[1-{*N'*-Cyano-*N*-[6-(difluoromethoxy)pyridin-2-yl]carbamimidoyl}-3-(3,4-dichlorophenyl)-4,5-dihydro-1*H*-pyrazol-4-yl]-*N*-ethyl-2-hydroxyacetamide (**32**). Compound **32** was prepared as described for **4**, starting from **11q** (1.9 g, 3.6 mmol). **32** was obtained as pale yellow solid (558 mg, 29 % over 3 steps). ¹H NMR (400 MHz, [D]₆DMSO): δ = 1.08 (br t, *J* = 7.1 Hz, 3H), 3.32–3.50 (m, 2H), 3.93–4.17 (m, 3H), 4.41 (br t, *J* = 11.7 Hz, 1H), 4.76 (br s, 1H), 6.84 (d, *J* = 8.2 Hz, 1H), 7.16 (br d, *J* = 8.2 Hz, 1H), 7.26 (t, *J* = 65.9 Hz, 1H), 7.63 (s, 1H), 7.75 (br d, *J* = 8.2 Hz, 1H), 7.94 (t, *J* = 8.0 Hz, 1H), 8.04 (s, 1H), 10.52 (br s, 1H). LC-MS (ESI): *m/z* = 526.1 [M + H]⁺.

Compound **32** was separated into its enantiomers by chiral SFC (instrument: Sepiatec Prep SFC 100, column: Chiralpak ID 5 μm, 250 × 20 mm, eluent: CO₂/*i*-PrOH 71:29, flow: 80 mL/min, temperature: 40 °C): *t*R (min) = 3.5–5.0 [(*R*)-**32**], 5.0–7.0 [(*S*)-**32**]. Enantiomer (*S*)-**32**: SFC (Chiralpak ID 5 μm, 100 × 4.6 mm, CO₂/*i*-PrOH 71:29, 4.0 mL/min): *t*R (min) = 3.82. [α]_D –56.2 (*c* 0.53, MeOH).

N-[1-{*N*-[4-Chloro-3-(difluoromethoxy)phenyl]-*N'*-cyanocarbamidoyl}-3-(3,4-dichlorophenyl)-4,5-dihydro-1*H*-pyrazol-4-yl]-*N*-ethyl-2-hydroxyacetamide (**33**). Compound **33** was prepared as described for **4**, starting from **11r** (1.5 g, 2.7 mmol). **33** was obtained as yellow solid (18 mg, 12 % over 3 steps). ¹H NMR (400 MHz, [D]₆DMSO): δ = 0.81 (br s, 1H), 0.99 (br s, 3H), 2.92 (br s, 0.4H), 3.01–3.29 (m, 3H), 3.94–4.33 (m, 6H), 4.40 (br s, 0.4H), 4.72

(t, $J = 5.3$ Hz, 1H), 5.13 (br s, 0.3H), 5.73 (br s, 0.4H), 5.94 (br s, 1H), 6.93–7.42 (m, 6H), 7.52–7.72 (m, 3H), 7.86–7.96 (m, 1H). LC-MS (ESI): $m/z = 559.2$ $[M + H]^+$.

Compound **33** was separated into its enantiomers by chiral SFC (instrument: Sepiatec Prep SFC 100, column: Chiralpak IC 5 μ m, 250 \times 20 mm, eluent: CO₂/EtOH 7:3, flow: 80 mL/min, temperature: 40 °C): t_R (min) = 4.75–5.6 [(*S*)-**33**], 6.25–7.5 [(*R*)-**33**]. Enantiomer (*S*)-**33**: SFC (Chiralpak IC 5 μ m, 100 \times 4.6 mm, CO₂/EtOH 7:3, 4.0 mL/min): t_R (min) = 2.99. $[\alpha]_D -37.4$ (c 1.0, DMSO).

N-[1-{*N'*-Cyano-*N*-[3-(difluoromethoxy)-5-fluorophenyl]carbamimidoyl}-3-(3,4-dichlorophenyl)-4,5-dihydro-1*H*-pyrazol-4-yl]-*N*-ethyl-2-hydroxyacetamide (**34**). Compound **34** was prepared as described for **4**, starting from **11s** (415 mg, 0.8 mmol). **34** was obtained as white solid (65 mg, 15 % over 3 steps). ¹H NMR (400 MHz, [D]₆DMSO): δ = 1.08 (br t, 3H), 3.39 (m, 1H), 4.00–4.20 (m, 3H), 4.50 (br t, $J = 11.5$ Hz, 1H), 4.77 (br t, $J = 5.8$ Hz, 1H), 5.59–6.16 (m, 1H), 6.95 (br d, $J = 8.1$ Hz, 1H), 7.10 (br s, 1H), 7.19 (br d, $J = 10.4$ Hz, 1H), 7.31 (t, $J = 73.5$ Hz, 1H), 7.66 (br d, $J = 8.4$ Hz, 1H), 7.77 (d, $J = 8.4$ Hz, 1H), 8.11 (s, 1H), 9.94 (br s, 1H). LC-MS (ESI): $m/z = 543.2$ $[M + H]^+$.

Compound **34** was separated into its enantiomers by chiral HPLC (instrument: Agilent Prep 1200, column: Chiralpak ID 5 μ m, 250 \times 30 mm, eluent: hexane/EtOH/Et₂NH 70:30:0.1, flow: 40 mL/min, temperature: 23 °C): t_R (min) = 6.5–7.7 [(*S*)-**34**], 8.1–9.7 [(*R*)-**34**]. Enantiomer (*S*)-**34**: HPLC (Chiralpak ID, 3 μ m, 100 \times 4.6 mm (hexane/EtOH/Et₂NH 70:30:0.1, 1.0 mL/min): t_R (min) = 3.81. $[\alpha]_D -38.1$ (c 1.0, DMSO).

Biology

Cell Culture. Cell lines were obtained from the American Type Culture Collection (HEK293, U2OS), the German Collection of Microorganisms and Cell Cultures (KYSE-150) and the European Collection of Cell Cultures (A2780). They were maintained in the recommended cell culture media at 37° C in 5% CO₂.

Enzyme Activity and Inhibition Assays. SMYD2 enzyme kinetics and inhibitory activities of compounds were analyzed using a scintillation proximity assay (SPA) which measured methylation by the enzyme of the synthetic, biotinylated peptide Btn-Ahx-GSRAHSSHLKSKKGQSTSRH-amide (Biosyntan) derived from the C-terminal domain of p53. The SMYD2 full-length enzyme with an N-terminal 6xHis tag was expressed in *E. coli* and purified by affinity chromatography on a Ni-NTA Sepharose column, followed by size-exclusion chromatography on a Superdex 200 16/60 column (GE Healthcare). Assays were conducted in 384-well microtiter plates in a buffer containing 50 mM Tris/HCl pH 9.0, 1 mM DTT, 0.01% (w/v) BSA and 0.0022% (v/v) Pluronic, and a final volume of 5 µL. The SMYD2 concentration in the assay was 3 nM, while tritiated *S*-adenosyl-L-methionine (³H-SAM) and the peptide substrate were present at 60 nM and 1 µM, respectively, to ensure “balanced” conditions.⁴⁶ Apparent Michaelis–Menten constants for SAM and the p53 peptide were determined by titrating one substrate to saturation at co-substrate concentrations of $1 \times K_{m(\text{app})}$. Enzyme kinetics were followed over 2 h by quenching the reactions as described above at time points 0, 5, 10, 15, 30, 60, 90 and 120 min. Compounds were tested in 11-point, 3.5-fold dilution series ranging from 0.1 nM to 20 µM. Reactions were run for 30 min and quenched by adding Streptavidin PS SPA imaging beads (Perkin-Elmer) to a concentration of 3.12 µg/µL, and 25 µM “cold” SAM. The amount of product was evaluated using a Viewlux (Perkin-Elmer) CCD plate imaging device [emission filter 613/55]. The data were normalized using two sets of control wells for high (=

enzyme reaction with DMSO instead of test compound = 0% = minimum inhibition) and low (= all assay components without enzyme = 100% = maximum inhibition) SMYD2 activity. IC₅₀ values were calculated by fitting the normalized inhibition data to a four-parameter logistic equation using either a Bayer proprietary tool or Genedata Screener analysis software.

For mechanism-of-inhibition studies, IC₅₀ determinations were basically performed as described above, but incubation times were adjusted to guarantee kinetic linearity at each concentration of substrate analyzed. For peptide competition studies, IC₅₀ values were determined at six different concentrations of p53 peptide (0.5, 1, 2, 4, 6 and 12 μM). For SAM competition, 25, 50, 100, 200, 300 and 600 nM ³H-SAM were used. In both cases, the other co-substrate was used at a concentration of 1 × K_{m(app)}.

Calculation of K_{i(app)} and αK_{i(app)} using the corresponding Cheng–Prusoff equations:⁴¹

$$K_{i(app)} = \frac{IC_{50}}{([S]/K_{m(app)} + 1)}$$

$$\alpha K_{i(app)} = \frac{IC_{50}}{(K_{m(app)}/[S] + 1)}$$

where [S]=substrate concentration, K_{m(app)} = apparent Michaelis–Menten constant, K_{i(app)} = apparent inhibitor constant for binding to free enzyme, and αK_{i(app)} = apparent inhibitor constant for binding to enzyme–substrate complex.

Selectivity Assays. The effect of (S)-4 on the methyltransferase activity of G9A, EHMT1, SUV39H1, SUV39H2, SETDB1, SETD7, SETD8, SUV420H1, SUV420H2, PRMT1, PRMT3, PRMT6, PRMT8, PRDM9, SETD2 and SMYD3, and MLL1, MLL3, EZH2 and PRMT5 complexes, as well as DNMT1 and BCDIN3D, was assessed using the SPA method.²⁸ For

DNMT3A/3L, DNMT3B/3L, ASH1L, DOT1L, NSD1, NSD2, NSD3, METTL21A, and METTL21D a trichloroacetic acid (TCA) precipitation method in filter plates were employed.⁴⁷

PAR1 Assay. The identification of PAR1 antagonistic effects and the quantification of those effects, as well as the resulting IC₅₀ values, were performed as described previously.³⁶

Biophysical Validation by ITC/TSA. Thermal shift assays (TSA) were carried out with the ThermoFluor system (Johnson & Johnson Pharmaceutical Research & Development). Melting curves were obtained at a protein concentration of 1.5 μ M, 8xSypro Orange (Invitrogen) and a ligand concentration of 100 μ M, using buffer containing 20 mM Tris pH 8.0, 100 mM NaCl, 8.5%. Scans were measured from 25 to 95 °C at a scanning rate of 2 °C/min. TSA data were analyzed using ThermoFluor++ (version 1.3.7) software.

Isothermal titration calorimetry (ITC) measurements were carried out using a MicroCal iTC200 system. In the experiments, compound (400 μ M) was titrated into SMYD2 protein (67 μ M) dissolved in 25 mM Tris pH 8.5, 50 mM NaCl, 0.0022% Pluronic F-127 and 2% DMSO at 25 °C. After an initial injection of 0.2 μ L, which was not considered for data fitting, 10 injections of 4 μ L each, in 150 s intervals were performed. The stirring speed of the protein in the cell was 500 rpm. The protein concentration was determined from UV absorbance measurements at 280 nm. Data were evaluated using ORIGIN software, as supplied with the instrument.

Purification and Crystallization of SMYD2. Recombinant human SMYD2 (UniProt Q9NRG4, amino acids 2–433) was expressed in insect cells (Sf9) containing an N-terminal TEV-cleavable 6xHis tag. Cell pellets were re-suspended in lysis buffer (40 mM Tris pH 8, 500 mM NaCl, 0.1% IGEPAL, 5 mM imidazole, 1 mM DTT) supplemented with complete EDTA-free protease inhibitor tablets and 50 U/mL Benzonase. The cell lysate was loaded onto a Ni-NTA column,

1
2
3 eluted with imidazole and concentrated using an ultracentrifugal filter unit. Then, SMYD2 was
4
5 gel-filtrated on a Superdex S200 column equilibrated in 20 mM Tris pH 8, 100 mM NaCl, 5%
6
7 glycerol and 1 mM DTT. The 6xHis tag was cleaved with TEV protease in solution at 6 °C
8
9 overnight. Uncleaved SMYD2 and TEV protease were separated from the cleaved product by a
10
11 second Ni-NTA affinity step. The cleaved SMYD2 protein was further purified by a second gel-
12
13 filtration step using a Superdex 200 column equilibrated in 20 mM Tris pH 8, 150 mM NaCl, 5%
14
15 glycerol and 1 mM Tris(2-carboxyethyl)phosphine (TCEP). The protein was concentrated to
16
17 15.5 mg/mL (313 μ M) (UV-vis) using an ultracentrifugal filter unit and shock-frozen in liquid
18
19 nitrogen. For crystallization, the cofactor SAM was added to a final concentration of 3.8 mM as
20
21 follows: SAM stock solution (100 mM in DMSO, 1.2 μ L) was added to concentrated SMYD2
22
23 solution (30 μ L) and incubated at 4 °C for 2 h. Crystals grew at 20 °C within 3 d using the
24
25 hanging drop method. Drops were made from the SMYD2/SAM solution (1 μ L) and reservoir
26
27 solution [20–24% (w/v) PEG 3350, 100 mM HEPES pH 7.0; 0.8 μ L]. 30 min after drop setup, a
28
29 seed solution (0.2 μ L) was added. The seed solution was made from SMYD2:SAM crystals
30
31 (obtained with the same reservoir conditions in a previous experiment) which were crashed
32
33 manually (using Seed Beads, Hampton Research), diluted in reservoir solution, shock-frozen and
34
35 stored at –80 °C. For complex formation, a crystal was transferred into a new drop reservoir
36
37 solution (1.5 μ L). A stock solution of the respective inhibitor (100 mM in DMSO) was 10-fold
38
39 diluted with reservoir solution. Over the course of 2 h, this diluted stock solution (1.5 μ L) was
40
41 added in three steps of 0.5 μ L to the drop containing the SMYD2:SAM crystal, resulting in a
42
43 final concentration of 5 mM inhibitor in the soaking drop. The crystal was soaked in this drop at
44
45 20 °C for 4 days in case of (*S*)-**4** and for 1 h for compound **6**.
46
47
48
49
50
51
52
53
54
55
56
57
58
59
60

Crystallographic Data Collection, Structure Determination and Refinement. The soaked crystal was briefly immersed in cryo buffer (0.1 M HEPES pH 7.0, 22% PEG 3350, 20% glycerol, 2 mM inhibitor) and shock-frozen in liquid nitrogen. Diffraction data sets were collected using beamline 14.1 at the Helmholtz-Zentrum Berlin at 100 K using a wavelength of 0.91841 Å and a PILATUS detector. The diffraction images were processed using the program XDS.⁴⁸ The crystals belonged to space group $P2_12_12_1$ with one molecule per asymmetric unit. The crystal form described here was first solved for an SMYD2:SAM crystal in the absence of an inhibitor, using the Molecular Replacement method (program *Phaser*⁴⁹ from the *CCP4* program suite⁵⁰ and PDB entry 3TG5 as search model). The data sets described here were then solved by rigid body refinement using the SMYD2:SAM structure as starting model and the program Refmac⁵¹ from the *CCP4* program suite. 3D models for compound **6** and (*S*)-**4** were generated using the program Discovery Studio, and parameter files for crystallographic refinement and model building were generated using the software *PRODRG*.⁵² (*S*)-**4** was manually built into the electron-density maps using Coot,⁵³ followed by several cycles of refinement with Refmac and rebuilding in Coot. For the data collection and refinement statistics, see Supporting Information Table S3.

WaterMap Calculations. WaterMap calculations were based on the crystal structure of the 4-chlorophenyl derivative **6** (PDB code 5ARF). The SMYD2–compound **6** complex structure was prepared using the Protein Preparation Wizard functionality in Maestro.^{54–57} Preparation involved assignment of bond orders, addition of hydrogens, creation of zero-order bonds to metals, deletion of water molecules beyond 5 Å from heteroatoms, assignment of protonation states according to pH 7.0, and optimization of the hydrogen-bonding network and restrained

minimization. Here, and for all further minimizations and simulations, the OPLS 2005 force field^{58, 59} was used.

Water sites and corresponding free energies were calculated using WaterMap.^{39,40} The calculation involved the following (default) settings: water molecules within 10 Å of the ligand were investigated, the ligand as well as any crystallographic water molecules were removed prior to simulation, the protein was truncated beyond 20 Å from the ligand and the simulation time was 2 ns. In brief (see ref⁴⁰ for details), the different stages of the calculation were solvation of the system in an orthorhombic box of TIP4P water⁶⁰ with a minimum distance between box edge and solute of 10 Å, and a series of minimizations and short simulations to equilibrate the system, followed by a 2-ns production simulation. All non-water heavy atoms were harmonically restrained during all minimizations and simulations using a force constant of 5 kcal mol⁻¹ Å⁻². Coordinates were saved every 1.5 ps, yielding a total of 1334 snapshots for further analysis. Water molecules were subsequently clustered such that non overlapping spheres (i.e., hydration sites) with radius 1 Å were obtained. Thermodynamic properties of these sites (i.e., enthalpies, entropies and thus free energies) were approximated as follows: Enthalpies were estimated as the difference between the average interaction energy of the water molecule with the rest of the system and the average interaction energy in bulk water. Entropies were estimated using inhomogeneous solvation theory.⁶¹

Antibody Generation. To detect SMYD2-mediated methylation, we used a lysine monomethylation specific rabbit polyclonal antibody (SY46). The antibody was generated (Eurogentec) against a p53 peptide containing the monomethylated K370 epitope, as described

elsewhere.¹³ Antibody has been purified against unmethylated p53 peptide. Using this antibody in cellular systems revealed that it also recognized methylated AHNAK which is also methylated by SMYD2 (see supplementary Figure S2).

In Vitro Methylation of Recombinant p53. Recombinant p53 protein (BD Pharmingen no. 556439) was incubated with full-length SMYD2 protein (in-house production) and SAM in reaction buffer (50 mM Tris pH 9, 1 mM DTT, 0.01% BSA, 0.0022% Pluronic) at 30 °C overnight.

Western Blot. Cells were lysed in RIPA buffer Pierce (Thermo Fisher Scientific) with Benzonase (Merck) and protease inhibitors (Roche Diagnostics). Proteins were separated by SDS-PAGE and blotted onto nitrocellulose membranes (Invitrogen). Membranes were blocked in 5% milk PBS-T (phosphate buffered saline with 0.1% Tween 20) and immunoprobed with antibodies raised against histone H3 (Cell Signaling Technology #4499S), p53 (BD Biosciences #554294), AHNAK (Santa Cruz Biotechnology, #sc-390743, 1:500), SMYD2 (abcam, #ab108217, 1:1000), beta-actin (abcam, #ab8224, 1:1000), or with the methylation specific antibody SY46 (Eurogentec). The secondary antibodies used were goat anti-mouse/rabbit IRDye 800 CW (LI-COR Biosciences) and Alexa Fluor 680 goat anti-mouse/rabbit IgG. Bands were detected and quantified with Odyssey Fc Software (LI-COR Biosciences). Western blot assay for p53 methylation in HEK293T cells was performed as described elsewhere with an antibody directed against p53K370me1 kindly provided by Dr. Shelley Berger.^{13, 28}

Caspase 3/7 Activation Assay. Effects on apoptosis induction were measured with the Caspase-Glo 3/7 Assay System (Promega). In brief, 10000 cells/well were treated for 2 d with compound **25** or (*S*)-**4** (to allow for demethylation of p53). Then, caspase activation was induced by

doxorubicin (Sigma) (1.25 μ M for U2OS and A2780 cells, 2.5 μ M for KYSE-150 cells) treatment for 24 h. The apoptotic index was determined by normalization of caspase 3/7 activation signals to proliferation effects, measured by alamarBlue (Thermo Fisher Scientific).

Cell-Based Assay for the Detection of SMYD2 Methylation Activity. For the detection of SMYD2 cellular methylation activity, an In-Cell Western (ICW) assay was established. For the ICW KYSE-150 cells stably transfected with a construct expressing wild-type N-terminal 2xc-myc-tagged SMYD2 (NCBI Reference Sequence: NP_064582.2) were used. For further detection and validation experiments of AHNAK methylation we additionally generated stable HeLa and MDA-MB-231 cell lines using the same construct. For conducting the ICW assay, 5000 SMYD2-engineered KYSE-150 cells/well were seeded in 96-well plates (Sigma) and cultivated for 24 h at 37° C in 5% CO₂. Nontransfected KYSE-150 cells were used as a control for maximal inhibition of methylation activity. Cells were grown in 49% RPMI 1640 and 49% Ham's F12 media supplemented with 2% heat-inactivated FCS. For the determination of SMYD2 inhibitory activity, cells were treated for 72 h in the presence of test compound (at a final concentration range of 3.9×10^{-8} to 5×10^{-6} M) or with DMSO. Media were removed and 3.7% (w/v) formaldehyde in PBS was added, for 20 min. After two washes with PBS, 0.25% (v/v) Triton X-100 in PBS was added, for 15 min of permeabilization. After one wash with PBS, cells were blocked in 5% (w/v) nonfat dry milk in PBS for 1 h. Fixed cells were exposed to primary methylation antibody (SY46, 1:200) in 5% nonfat dry milk in PBS for 24 h. One row of cells on each plate was not exposed to methylation antibody (SY46) and was reserved for background control measurements. The wells were washed three times with PBS, then secondary IR800-conjugated antibody (LI-COR, # 926-32211, 1:1000) and DNA-intercalating dye DRAQ5 (Thermo Fisher Scientific, # 62251, 1:1000) were added for 3 h in blocking buffer. After five

washes with PBS, the fluorescence in each well was measured on an Odyssey scanner (LI-COR) at 800 nm (SY46 methylation signal, 764 nm excitation) and 700 nm (DRAQ5 signal, 683 nm excitation). Fluorescence intensity was quantified and normalized to background and DRAQ5 signals. The normalized data were further analyzed by four-parameter logistic regression analysis using a Bayer proprietary tool to determine the IC₅₀ value for each tested compound. For IC₅₀ determinations, C₀ (= no inhibition) was defined as the signal measured for the DMSO-treated controls. C_i (maximal inhibition) was defined as the signal measured for nontransfected KYSE-150 cells.

Proliferation Panel. For the characterization of proliferation effects, the OncoPanel 240 (Eurofins Panlabs) was used.

Mouse Tumor Xenograft Model. Animal experiments were conducted in accordance with the German animal welfare laws, approved by local authorities, and in accordance with the ethical guidelines of Bayer AG. 8-week-old female BALB/c nude mice obtained from Charles River Laboratories (Germany) were acclimated for at least for 24 h before tumor cell injection. KYSE-150 cells (4×10^6) were re-suspended in 100% Matrigel (100 μ L) and injected subcutaneously into the right flank region of the mice; 4 days after tumor cell inoculation, mice were randomized into four treatment groups. Treatment was started at day 4 after tumor inoculation. Group 1 (n = 12) was treated with vehicle only (Solutol/ethanol/water 1:1:8) iv q.d. and once at day 4 with saline iv; Group 2 (n = 6) was treated with 500 mg/kg (S)-4 po q.d.; Group 3 (n = 12) was treated with 10 mg/kg doxorubicin iv once at day 4; Group 4 (n = 6) was treated with a combination of (S)-4 and doxorubicin. Tumors were measured three times per week for 14 days. Tumor weight is assumed to be lognormally distributed, thus, all tumor weights were logarithmically transformed (base = 2) prior to statistical inference. One-sided Dunnett's

comparison of log₂ tumor weights of all treatment groups with the vehicle group were carried out on an overall significance level of 0.05. The results were transformed from the log₂ scale to the original scale so that the difference from the pairwise comparisons and the respective 95% confidence intervals calculated on the log₂ scale correspond to T/C ratios of geometric mean values plus respective 95% confidence intervals on the original tumor weight scale (mg). Data was analyzed with R 3.0.1.

Ex Vivo Methylation Detection by Dot Blot. 8-week-old female BALB/c nude mice obtained from Charles River Laboratories (Germany) were acclimated for at least for 24 h before tumor cell injection. SMYD2-engineered KYSE-150 cells (4×10^6) were re-suspended in 100% Matrigel (100 μ L) and injected subcutaneously into the right flank region of the mice. Treatment was started when tumors reached a tumor area of 60–70 mm² (day 7 after inoculation). Mice (n = 12 per group) were treated with 10, 30, 70 or 100 mg/kg (S)-4 po q.d. for 3 d, or vehicle (PEG 400/water 8:2) po q.d. for 3 d. After the treatment period, tumor samples were immediately frozen in liquid nitrogen and stored at –80 °C. Frozen tumors were mechanically homogenized using TissueLyser and stainless steel beads (Qiagen), and proteins were extracted as described for the western blot method. Whole protein lysate (50 μ g per sample) was transferred with the Dot-Blot System MiniFold-1 (Whatman) onto a nitrocellulose membrane (Invitrogen). Membrane were blocked in 5% milk PBS-T and immunoprobed with the SY46 methylation antibody. The secondary antibody used was goat anti-rabbit IRDye 800 CW (LI-COR , #926-32211, 1:1000). Bands were detected and quantified with Odyssey Fc Software (LI-COR Biosciences).

In Vivo Rat PK. Pharmacokinetic properties of (*S*)-4 were determined by administering the test compound as indicated. Blood samples were withdrawn at different time points and plasma was separated by centrifugation. The samples were analyzed by LC-MS/MS.

Metabolic Stability in Rat Hepatocytes. Liver cells were distributed in Williams' medium E containing 5% fetal calf serum (FCS) to glass vials at a density of 1.0×10^6 vital cells/mL. The test compound was added to a final concentration of 1 μ M. During incubation, the hepatocyte suspensions were continuously shaken and aliquots were taken at 2, 8, 16, 30, 45 and 90 min, to which an equal volume of cold MeOH was immediately added. Samples were frozen at -20°C overnight, then centrifuged (15 min, 3000 rpm) and the supernatant was analyzed with an Agilent 1200 HPLC system with LC-MS/MS detection. The half-life of a test compound was determined from the concentration–time plot. The intrinsic clearances were calculated from the half-life, together with additional parameters (liver blood flow, quantity of liver cells in vivo and in vitro). The hepatic in vivo blood clearance (CL) and the maximal oral bioavailability (F_{max}) were calculated using the following parameters: liver blood flow: 4.2 L/h/kg rat, specific liver weight: 32 g/kg rat body weight, liver cells in vivo: 1.1×10^8 cells/g liver, liver cells in vitro: 0.5×10^6 /mL.

Caco2 Drug Permeability Assay. Caco-2 cells (purchased from DSMZ Braunschweig, Germany) were seeded at a density of 4.5×10^4 cell per well on 24 well insert plates, 0.4 μ m pore size, and grown for 15 days in DMEM medium supplemented with 10% fetal bovine serum, 1% GlutaMAX (100x, GIBCO), 100 μ g/ml penicillin, 100 μ g/ml streptomycin (GIBCO) and 1% nonessential amino acids (100 x). Cells were maintained at 37°C in a humidified 5% CO_2 atmosphere. Medium was changed every 2nd to 3rd day. Before running the permeation assay, the culture medium was replaced by an FCS-free hepes-carbonate transport buffer (pH 7.2). For

assessment of monolayer integrity the transepithelial electrical resistance (TEER) was measured. Test compounds were dissolved in DMSO and added either to the apical or basolateral compartment in final concentration of 2 μ M. Before and after incubation at 37 $^{\circ}$ C samples were taken from both compartments. Analysis of compound content was performed following precipitation with methanol and LC/MS/MS analysis. Permeability (P_{app}) was calculated in the apical to basolateral (A \rightarrow B) and basolateral to apical (B \rightarrow A) directions. The apparent permeability was calculated using following equation:

$$P_{app} = (V_r/P_o)(1/S)(P_2/t)$$

where V_r = volume of medium in the receiver chamber, P_o = measured peak area of the test drug in the donor chamber at $t = 0$, S = surface area of the monolayer, P_2 = measured peak area of the test drug in the acceptor chamber after incubation for 2 h, and t = incubation time. The efflux ratio basolateral (B) to apical (A) was calculated by dividing P_{app} (B–A) by P_{app} (A–B). In addition, the compound recovery was calculated. Reference compounds were analyzed in parallel as assay controls. All samples were analyzed by LC/MS/MS.

ASSOCIATED CONTENT

*S Supporting Information

Additional figure and tables of PK and exposure data, selectivity data, and crystallographic data collection and refinement statistics.

Accession Codes

The coordinates and structure factors for the described crystal structures have been deposited with the Protein Data Bank (PDB). The PDB accession codes are 5ARF (compound **6**) and 5ARG (*S*)-4.

AUTHOR INFORMATION

Corresponding Authors

*E-mail: carlo.stresemann@bayer.com; timo.stellfeld@bayer.com. Phone: (+49)3046812866, (+49)3046815727.

Notes

The authors declare the following competing financial interest(s): T.S., E.E., R.C.H, S.K., D.S., J.W., N.B., J.M., C.D.C, A.t.L., T.L., A.E.F.-M, V.B., H. W., I.V.H., and C.S. are or have been employees and stockholders of Bayer AG.

ACKNOWLEDGMENTS

We thank Peakdale Molecular Ltd. UK for excellent support in chemistry, Dr. Shelley Berger for providing p53 antibody. Beamline scientists at the Helmholtz-Zentrum Berlin for excellent facilities and support during data collection, moloX GmbH for crystallographic data collection,

and Hanspeter Lauble for help with crystallographic refinement. The SGC is a registered charity (number 1097737) that receives funds from AbbVie, Bayer Pharma AG, Boehringer Ingelheim, Canada Foundation for Innovation, Eshelman Institute for Innovation, Genome Canada, Innovative Medicines Initiative (EU/EFPIA) [ULTRA-DD grant no. 115766], Janssen, Merck & Co., Novartis Pharma AG, Ontario Ministry of Economic Development and Innovation, Pfizer, São Paulo Research Foundation-FAPESP, Takeda, and the Wellcome Trust.

ABBREVIATIONS USED

SMYD2, SET and MYND domain containing 2; SET domain, was first recognized as a conserved sequence in three *Drosophila melanogaster* proteins: a modifier of position-effect variegation, Suppressor of variegation 3-9 (Su(var)3-9), the Polycomb-group chromatin regulator Enhancer of zeste (E(z)), and the trithorax-group chromatin regulator trithorax (Trx); MYND domain, (myeloid, Nervy, and DEAF-1); ESCC, esophageal squamous carcinoma; HSP90a, Heat shock protein HSP 90-alpha 1; PARP1, Poly(ADP-ribose)-Polymerase 1; TSA, Thermal shift assay; ITC, Isothermal titration calorimetry; NCBI, National Center for Biotechnology Information; CCD, charge-coupled device; HEPES, (4-(2-hydroxyethyl)-1-piperazineethanesulfonic acid; FCS, fetal calf serum; SAM, S-adenosyl-L-methionine; PRMT5, protein arginine methyltransferase 5; G9A, euchromatic histone-lysine N-methyltransferase 2; EHMT1, euchromatic histone-lysine N-methyltransferase 1; SUV39H1, suppressor of variegation 3-9 homolog 1; SUV39H2, suppressor of variegation 3-9 homolog 2; SETDB1, SET domain bifurcated 1; SETD7, SET domain containing (lysine methyltransferase) 7; SETD8, SET domain containing (lysine methyltransferase) 8; SUV420H1, suppressor of variegation 4-20 homolog 1; SUV420H2, suppressor of variegation 4-20 homolog 2; PRMT1, protein arginine methyltransferase 1; PRMT3, protein arginine methyltransferase 3; PRMT6, protein arginine

1
2
3
4
5
6
7
8
9
10
11
12
13
14
15
16
17
18
19
20
21
22
23
24
25
26
27
28
29
30
31
32
33
34
35
36
37
38
39
40
41
42
43
44
45
46
47
48
49
50
51
52
53
54
55
56
57
58
59
60

methyltransferase 6; PRMT8, protein arginine methyltransferase 8; PRDM9, PR domain 9; SETD2, SET domain containing 2; SMYD3, SET and MYND domain containing 3; MLL1, lysine methyltransferase 2A; MLL3, lysine methyltransferase 2C; EZH2, enhancer of zeste 2 polycomb repressive complex 2 subunit; DNMT1, DNA (cytosine-5-)-methyltransferase; BCDIN3D, BCDIN3 domain containing RNA methyltransferase; DNMT3A, DNA (cytosine-5-)-methyltransferase 3 alpha; DNMT3B, DNA (cytosine-5-)-methyltransferase 3 beta; DNMT3L, DNA (cytosine-5-)-methyltransferase 3-like; ASH1L, ash1 (absent, small, or homeotic)-like; DOT1L, DOT1 like histone H3K79 methyltransferase; NSD1, nuclear receptor binding SET domain protein 1; NSD2, Wolf-Hirschhorn syndrome candidate 1; NSD3, Wolf-Hirschhorn syndrome candidate 1-like 1; METTL21A, methyltransferase like 21A; METTL21D, valosin containing protein lysine methyltransferase; T/C; treatment/control group;

REFERENCES

- (1) Zhang, X.; Huang, Y.; Shi, X. Emerging roles of lysine methylation on non-histone proteins. *Cell. Mol. Life Sci.* **2015**, *72*, 4257–4272.
- (2) Komatsu, S.; Imoto, I.; Tsuda, H.; Kozaki, K.-i.; Muramatsu, T.; Shimada, Y.; Aiko, S.; Yoshizumi, Y.; Ichikawa, D.; Otsuji, E.; Inazawa, J. Overexpression of SMYD2 relates to tumor cell proliferation and malignant outcome of esophageal squamous cell carcinoma. *Carcinogenesis* **2009**, *30*, 1139–1146.
- (3) Komatsu, S.; Ichikawa, D.; Hirajima, S.; Nagata, H.; Nishimura, Y.; Kawaguchi, T.; Miyamae, M.; Okajima, W.; Ohashi, T.; Konishi, H.; Shiozaki, A.; Fujiwara, H.; Okamoto, K.; Tsuda, H.; Imoto, I.; Inazawa, J.; Otsuji, E. Overexpression of SMYD2 contributes to malignant outcome in gastric cancer. *Br. J. Cancer* **2015**, *112*, 357–364.
- (4) Cho, H.-S.; Hayami, S.; Toyokawa, G.; Maejima, K.; Yamane, Y.; Suzuki, T.; Dohmae, N.; Kogure, M.; Kang, D.; Neal, D. E.; Ponder, B. A. J.; Yamaue, H.; Nakamura, Y.; Hamamoto, R. RB1 methylation by SMYD2 enhances cell cycle progression through an increase of RB1 phosphorylation. *Neoplasia* **2012**, *14*, 476–486.
- (5) Sakamoto, L. H.; Andrade, R. V.; Felipe, M. S.; Motoyama, A. B.; Pittella Silva, F. SMYD2 is highly expressed in pediatric acute lymphoblastic leukemia and constitutes a bad prognostic factor. *Leuk. Res.* **2014**, *38*, 496–502.
- (6) Pimkhaokham, A.; Shimada, Y.; Fukuda, Y.; Kurihara, N.; Imoto, I.; Yang, Z.-Q.; Imamura, M.; Nakamura, Y.; Amagasa, T.; Inazawa, J. Nonrandom chromosomal imbalances in esophageal squamous cell carcinoma cell lines: possible involvement of the *ATF3* and *CENPF* genes in the 1q32 amplicon. *Jpn. J. Cancer Res.* **2000**, *91*, 1126–1133.

- (7) Brown, M. A.; Sims, R. J., 3rd; Gottlieb, P. D.; Tucker, P. W. Identification and characterization of Smyd2: a split SET/MYND domain-containing histone H3 lysine 36-specific methyltransferase that interacts with the Sin3 histone deacetylase complex. *Mol. Cancer* **2006**, *5*, 26.
- (8) Abu-Farha, M.; Lambert, J.-P.; Al-Madhoun, A. S.; Elisma, F.; Skerjanc, I. S.; Figeys, D. The tale of two domains: proteomics and genomics analysis of SMYD2, a new histone methyltransferase. *Mol. Cell. Proteomics* **2008**, *7*, 560–572.
- (9) Hamamoto, R.; Saloura, V.; Nakamura, Y. Critical roles of non-histone protein lysine methylation in human tumorigenesis. *Nat. Rev. Cancer* **2015**, *15*, 110–124.
- (10) Benayoun, B. A.; Veitia, R. A. A post-translational modification code for transcription factors: sorting through a sea of signals. *Trends Cell Biol.* **2009**, *19*, 189–197.
- (11) Fan, J.-D.; Lei, P.-J.; Zheng, J.-Y.; Wang, X.; Li, S.; Liu, H.; He, Y.-L.; Wang, Z.-N.; Wei, G.; Zhang, X.; Li, L.-Y.; Wu, M. The selective activation of p53 target genes regulated by SMYD2 in BIX-01294 induced autophagy-related cell death. *PLoS One* **2015**, *10*, e0116782.
- (12) Ferguson, A. D.; Larsen, N. A.; Howard, T.; Pollard, H.; Green, I.; Grande, C.; Cheung, T.; Garcia-Arenas, R.; Cowen, S.; Wu, J.; Godin, R.; Chen, H.; Keen, N. Structural basis of substrate methylation and inhibition of SMYD2. *Structure* **2011**, *19*, 1262–1273.
- (13) Huang, J.; Perez-Burgos, L.; Placek, B. J.; Sengupta, R.; Richter, M.; Dorsey, J. A.; Kubicek, S.; Opravil, S.; Jenuwein, T.; Berger, S. L. Repression of p53 activity by Smyd2-mediated methylation. *Nature* **2006**, *444*, 629–632.
- (14) Jiang, Y.; Sirinupong, N.; Brunzelle, J.; Yang, Z. Crystal structures of histone and p53 methyltransferase SmyD2 reveal a conformational flexibility of the autoinhibitory C-terminal domain. *PLoS One* **2011**, *6*, e21640.

- (15) Sajjad, A.; Novoyatleva, T.; Vergarajauregui, S.; Troidl, C.; Schermuly, R. T.; Tucker, H. O.; Engel, F. B. Lysine methyltransferase Smyd2 suppresses p53-dependent cardiomyocyte apoptosis. *Biochim. Biophys. Acta* **2014**, *1843*, 2556–2562.
- (16) Wang, L.; Li, L.; Zhang, H.; Luo, X.; Dai, J.; Zhou, S.; Gu, J.; Zhu, J.; Atadja, P.; Lu, C.; Li, E.; Zhao, K. Structure of human SMYD2 protein reveals the basis of p53 tumor suppressor methylation. *J. Biol. Chem.* **2011**, *286*, 38725–38737.
- (17) Wu, J.; Cheung, T.; Grande, C.; Ferguson, A. D.; Zhu, X.; Theriault, K.; Code, E.; Birr, C.; Keen, N.; Chen, H. Biochemical characterization of human SET and MYND domain-containing protein 2 methyltransferase. *Biochemistry* **2011**, *50*, 6488–6497.
- (18) Barros Filho, M. C.; Katayama, M. L. H.; Brentani, H.; Abreu, A. P. S.; Barbosa, E. M.; Oliveira, C. T.; Góes, J. C. S.; Brentani, M. M.; Folgueira, M. A. A. K. Gene trio signatures as molecular markers to predict response to doxorubicin cyclophosphamide neoadjuvant chemotherapy in breast cancer patients. *Braz. J. Med. Biol. Res.* **2010**, *43*, 1225–1231.
- (19) Jiang, Y.; Trescott, L.; Holcomb, J.; Zhang, X.; Brunzelle, J.; Sirinpong, N.; Shi, X.; Yang, Z. Structural insights into estrogen receptor alpha methylation by histone methyltransferase SMYD2, a cellular event implicated in estrogen signaling regulation. *J. Mol. Biol.* **2014**, *426*, 3413–25.
- (20) Zhang, X.; Tanaka, K.; Yan, J.; Li, J.; Peng, D.; Jiang, Y.; Yang, Z.; Barton, M. C.; Wen, H.; Shi, X. Regulation of estrogen receptor alpha by histone methyltransferase SMYD2-mediated protein methylation. *Proc. Natl. Acad. Sci. U S A* **2013**, *110*, 17284–9

- (21) Piao, L.; Kang, D.; Suzuki, T.; Masuda, A.; Dohmae, N.; Nakamura, Y.; Hamamoto, R. The histone methyltransferase SMYD2 methylates PARP1 and promotes poly(ADP-ribosyl)ation activity in cancer cells. *Neoplasia* **2014**, *16*, 257–264.e2.
- (22) Abu-Farha, M.; Lanouette, S.; Elisma, F.; Tremblay, V.; Butson, J.; Figeys, D.; Couture, J.-F. Proteomic analyses of the SMYD family interactomes identify HSP90 as a novel target for SMYD2. *J. Mol. Cell. Biol.* **2011**, *3*, 301–308.
- (23) Hamamoto, R.; Toyokawa, G.; Nakakido, M.; Ueda, K.; Nakamura, Y. SMYD2-dependent HSP90 methylation promotes cancer cell proliferation by regulating the chaperone complex formation. *Cancer Lett.* **2014**, *351*, 126–133.
- (24) Donlin, L. T.; Andresen, C.; Just, S.; Rudensky, E.; Pappas, C. T.; Kruger, M.; Jacobs, E. Y.; Unger, A.; Zieseniss, A.; Dobenecker, M.-W.; Voelkel, T.; Chait, B. T.; Gregorio, C. C.; Rottbauer, W.; Tarakhovsky, A.; Linke, W. A. Smyd2 controls cytoplasmic lysine methylation of Hsp90 and myofilament organization. *Genes Dev.* **2012**, *26*, 114–119.
- (25) Voelkel, T.; Andresen, C.; Unger, A.; Just, S.; Rottbauer, W.; Linke, W. A. Lysine methyltransferase Smyd2 regulates Hsp90-mediated protection of the sarcomeric titin springs and cardiac function. *Biochim. Biophys. Acta* **2013**, *1833*, 812–822.
- (26) Bunnage, M. E.; Piatnitski Chekler, E. L.; Jones, L. H. Target validation using chemical probes. *Nat. Chem. Biol.* **2013**, *9*, 195–199.
- (27) Arrowsmith, C. H.; Audia, J. E.; Austin, C.; Baell, J.; Bennett, J.; Blagg, J.; Bountra, C.; Brennan, P. E.; Brown, P. J.; Bunnage, M. E.; Buser-Doepner, C.; Campbell, R. M.; Carter, A. J.; Cohen, P.; Copeland, R. A.; Cravatt, B.; Dahlin, J. L.; Dhanak, D.; Edwards, A. M.; Frederiksen, M.; Frye, S. V.; Gray, N.; Grimshaw, C. E.; Hepworth, D.; Howe, T.; Huber, K. V. M.; Jin, J.; Knapp, S.; Kotz, J. D.; Kruger, R. G.; Lowe, D.; Mader, M. M.; Marsden, B.;

Mueller-Fahrnow, A.; Müller, S.; O'Hagan, R. C.; Overington, J. P.; Owen, D. R.; Rosenberg, S. H.; Ross, R.; Roth, B.; Schapira, M.; Schreiber, S. L.; Shoichet, B.; Sundström, M.; Superti-Furga, G.; Taunton, J.; Toledo-Sherman, L.; Walpole, C.; Walters, M. A.; Willson, T. M.; Workman, P.; Young, R. N.; Zuercher, W. J. The promise and peril of chemical probes. *Nat. Chem. Biol.* **2015**, *11*, 536–541.

(28) Nguyen, H.; Allali-Hassani, A.; Antonysamy, S.; Chang, S.; Chen, L. H.; Curtis, C.; Emtage, S.; Fan, L.; Gheyi, T.; Li, F.; Liu, S.; Martin, J. R.; Mendel, D.; Olsen, J. B.; Pelletier, L.; Shatseva, T.; Wu, S.; Zhang, F. F.; Arrowsmith, C. H.; Brown, P. J.; Campbell, R. M.; Garcia, B. A.; Barsyte-Lovejoy, D.; Mader, M.; Vedadi, M. LLY-507, a cell-active, potent, and selective inhibitor of protein-lysine methyltransferase SMYD2. *J. Biol. Chem.* **2015**, *290*, 13641–13653.

(29) Sweis, R. F.; Wang, Z.; Algire, M.; Arrowsmith, C. H.; Brown, P. J.; Chiang, G. G.; Guo, J.; Jakob, C. G.; Kennedy, S.; Li, F.; Maag, D.; Shaw, B.; Soni, N. B.; Vedadi, M.; Pappano, W. N. Discovery of A-893, a new cell-active benzoxazinone inhibitor of lysine methyltransferase SMYD2. *ACS Med. Chem. Lett.* **2015**, *6*, 695–700.

(30) Structural Genomics Consortium, BAY-598 A selective chemical probe for SMYD2. <http://www.thesgc.org/chemical-probes/BAY-598> (accessed Mar 9, 2016).

(31) Reynoird, N.; Mazur, P. K.; Stellfeld, T.; Flores, N. M.; Lofgren, S. M.; Carlson, S. M.; Brambilla, E.; Hainaut, P.; Kaznowska, E. B.; Arrowsmith, C. H.; Khatri, P.; Stresemann, C.; Gozani, O.; Sage, J. Coordination of stress signals by the lysine methyltransferase SMYD2 promotes pancreatic cancer. *Genes Dev.* **2016**, *30*, 772–785.

(32) Hieda, Y.; Tsukita, S.; Tsukita, S. A new high molecular mass protein showing unique localization in desmosomal plaque. *J. Cell. Biol.* **1989**, *109*, 1511–1518.

- (33) Tarcsay, A.; Keserű, G. M. Is there a link between selectivity and binding thermodynamics profiles? *Drug Discovery Today* **2015**, *20*, 86–94.
- (34) Ladbury, J. E.; Klebe, G.; Freire, E. Adding calorimetric data to decision making in lead discovery: a hot tip. *Nat. Rev. Drug Discovery* **2010**, *9*, 23–27.
- (35) Macfarlane, S. R.; Seatter, M. J.; Kanke, T.; Hunter, G. D.; Plevin, R. Proteinase-activated receptors. *Pharmacol. Rev.* **2001**, *53*, 245–282.
- (36) Leger, A. J.; Covic, L.; Kuliopulos, A. Protease-activated receptors in cardiovascular diseases. *Circulation* **2006**, *114*, 1070–1077.
- (37) Allerheiligen, S.; Brohm, D.; Diedrichs, N.; Hübsch, W.; Fröhlen, B.-N.; Gerdes, C.; Gnoth, M. J.; Perzborn, E.; Vöhringer, V. (Bayer HeathCare AG). Cyanoguanidine-substituted pyrazolines. WO2006072350, 2006.
- (38) Abad-Zapatero, C.; Metz, J. T. Ligand efficiency indices as guideposts for drug discovery. *Drug Discovery Today* **2005**, *10*, 464–469.
- (39) *Schrödinger Suite 2012* Update2, WaterMap, version 1.4.518, Schrödinger LLC, New York, NY, **2012**
- (40) Young, T.; Abel, R.; Kim, B.; Berne, B. J.; Friesner, R. A. Motifs for molecular recognition exploiting hydrophobic enclosure in protein-ligand binding. *Proc. Natl. Acad. Sci. U S A* **2007**, *104*, 808–813.
- (41) Cheng, Y.; Prusoff, W. H. Relationship between the inhibition constant (K_1) and the concentration of inhibitor which causes 50 per cent inhibition (I_{50}) of an enzymatic reaction. *Biochem. Pharmacol.* **1973**, *22*, 3099–3108.
- (42) Copeland, R. A. Mechanistic considerations in high-throughput screening. *Anal. Biochem.* **2003**, *320*, 1–12.

- (43) Chan-Penebre, E.; Kuplast, K. G.; Majer, C. R.; Boriack-Sjodin, P. A.; Wigle, T. J.; Johnston, L. D.; Rioux, N.; Munchhof, M. J.; Jin, L.; Jacques, S. L.; West, K. A.; Lingaraj, T.; Stickland, K.; Ribich, S. A.; Raimondi, A.; Scott, M. P.; Waters, N. J.; Pollock, R. M.; Smith, J. J.; Barbash, O.; Pappalardi, M.; Ho, T. F.; Nurse, K.; Oza, K. P.; Gallagher, K. T.; Kruger, R.; Moyer, M. P.; Copeland, R. A.; Chesworth, R.; Duncan, K. W. A selective inhibitor of PRMT5 with in vivo and in vitro potency in MCL models. *Nat. Chem. Biol.* **2015**, *11*, 432–437.
- (44) Fabian, M. A.; Biggs, W. H., 3rd; Treiber, D. K.; Atteridge, C. E.; Azimioara, M. D.; Benedetti, M. G.; Carter, T. A.; Ciceri, P.; Edeen, P. T.; Floyd, M.; Ford, J. M.; Galvin, M.; Gerlach, J. L.; Grotzfeld, R. M.; Herrgard, S.; Insko, D. E.; Insko, M. A.; Lai, A. G.; Lelias, J. M.; Mehta, S. A.; Milanov, Z. V.; Velasco, A. M.; Wodicka, L. M.; Patel, H. K.; Zarrinkar, P. P.; Lockhart, D. J. A small molecule-kinase interaction map for clinical kinase inhibitors. *Nat. Biotechnol.* **2005**, *23*, 329–336.
- (45) Olsen, J. B., Cao, X. J., Han, B., Chen, L. H., Horvath, A., Richardson, T. I., Campbell, R. M., Garcia, B. A., and Nguyen, H. Quantitative profiling of the activity of protein lysine methyltransferase SMYD2 using SILAC-based proteomics, *Mol. Cell. Proteomics* **2016**, *15*, 892-905..
- (46) Yang, J.; Copeland, R. A.; Lai, Z. Defining balanced conditions for inhibitor screening assays that target bisubstrate enzymes. *J. Biomol. Screen.* **2009**, *14*, 111–120.
- (47) Eram, M. S., Kuznetsova, E., Li, F., Lima-Fernandes, E., Kennedy, S., Chau, I., Arrowsmith, C. H., Schapira, M., and Vedadi, M. Kinetic characterization of human histone H3 lysine 36 methyltransferases, ASH1L and SETD2, *Biochim. Biophys. Acta* **2015**, *1850*, 1842-1848.
- (48) Kabsch, W. Xds. *Acta Crystallogr., Sect. D: Biol. Crystallogr.* **2010**, *66*, 125–132.

- (49) McCoy, A. J.; Grosse-Kunstleve, R. W.; Adams, P. D.; Winn, M. D.; Storoni, L. C.; Read, R. J. Phaser crystallographic software. *J. Appl. Crystallogr.* **2007**, *40*, 658–674.
- (50) Winn, M. D.; Ballard, C. C.; Cowtan, K. D.; Dodson, E. J.; Emsley, P.; Evans, P. R.; Keegan, R. M.; Krissinel, E. B.; Leslie, A. G.; McCoy, A.; McNicholas, S. J.; Murshudov, G. N.; Pannu, N. S.; Potterton, E. A.; Powell, H. R.; Read, R. J.; Vagin, A.; Wilson, K. S. Overview of the CCP4 suite and current developments. *Acta Crystallogr., Sect. D: Biol. Crystallogr.* **2011**, *67*, 235–242.
- (51) Murshudov, G. N.; Vagin, A. A.; Dodson, E. J. Refinement of macromolecular structures by the maximum-likelihood method. *Acta Crystallogr., Sect. D: Biol. Crystallogr.* **1997**, *53*, 240–255.
- (52) Schüttelkopf, A. W.; van Aalten, D. M. PRODRG: a tool for high-throughput crystallography of protein-ligand complexes. *Acta Crystallogr., Sect. D: Biol. Crystallogr.* **2004**, *60*, 1355–1363.
- (53) Emsley, P.; Lohkamp, B.; Scott, W. G.; Cowtan, K. Features and development of Coot. *Acta Crystallogr., Sect. D: Biol.* **2010**, *66*, 486–501.
- (54) *Epik version 2.3.518*, Schrödinger, LLC, New York, NY, **2012**; .
- (55) *Impact version 5.8.518*, Schrödinger, LLC, New York, NY, **2012**; .
- (56) *Prime version 3.1.518*, Schrödinger, LLC, New York, NY, **2012**.
- (57) *Schrödinger Suite 2012 Update2*, Protein Preparation Wizard; .
- (58) Jorgensen, W. L.; Tirado-Rives, J. The OPLS [optimized potentials for liquid simulations] potential functions for proteins, energy minimizations for crystals of cyclic peptides and crambin. *J. Am. Chem. Soc.* **1988**, *110*, 1657–1666.

- 1
2
3 (59) Jorgensen, W. L.; Maxwell, D. S.; Tirado-Rives, J. Development and testing of the OPLS
4 all-atom force field on conformational energetics and properties of organic liquids. *J. Am. Chem.*
5 *Soc.* **1996**, *118*, 11225–11236.
6
7
8
9
10 (60) Jorgensen, W. L.; Chandrasekhar J.; Madura J. D.; Impey R. W.; Klein M. L. Comparison
11 of simple potential functions for simulating liquid water. *J. Chem. Phys.* **1983**, *79*, 926–935.
12
13 (61) Lazaridis, T. Inhomogeneous fluid approach to solvation thermodynamics. 1. Theory. *J.*
14 *Phys. Chem. B* **1998**, *102*, 3531–3541.
15
16
17
18
19
20
21
22
23
24
25
26
27
28
29
30
31
32
33
34
35
36
37
38
39
40
41
42
43
44
45
46
47
48
49
50
51
52
53
54
55
56
57
58
59
60

Figure captions

Figure 1. Comparison of so far described SMYD2 inhibitors with (*S*)-**4** discovered in this study.

Data from respective references as well as assay results from this study are presented.

Figure 2. Identification and biophysical validation of the pyrazoline SMYD2 inhibitor series leading to (*S*)-**4**. (A) Scintillation proximity assay (SPA) screening approach leading to the pyrazoline hit cluster, with representative hit compound **5** with $IC_{50} = 1.7 \mu M$. (B) Thermal shift assay (TSA) for SMYD2 protein stabilization for inhibitors of the aminopyrazoline series [**•**], with aminopyrazoline hit **5** ($\Delta T_m = 3.3 K$) and (*S*)-**4** ($\Delta T_m = 7.1 K$) highlighted. Stabilization correlates with SPA potency. (C) Isothermal titration calorimetry (ITC) of compound **6** indicating a submicromolar binding constant ($K_d = 540 nM$) and a high enthalpic contribution to the binding energy.

Figure 3. Binding mode of compound **6** and (*S*)-**4**. (A) and (B) Two different views of the co-crystal structure of **6** in complex with SMYD2. There is a good steric and electrostatic fit of **6** into the substrate binding site of SMYD2, and multiple hydrogen-bond interactions are involved. The lysine channel is occupied by the 4-chlorophenyl residue of the ligand, representing a novel lysine channel binding motif. In addition, pockets-1 and -2 are addressed. (C) Visualization of the WaterMap calculations suggesting an optimal displacement of water molecules by a 3,4-dichlorophenyl residue. Calculated water sites are shown as spheres and colored based on their free energy. Only sites within the lysine channel are shown. WaterMap results are based on the crystal structure of the monochloro derivative **6** (PDB code 5ARF). The protein surface is depicted in gray. The modeled ligand structure is shown as colored sticks (chlorine: green,

carbon: yellow, hydrogen: white, nitrogen: blue, oxygen: red, fluorine: light green). For clarity, protein residues and cofactors are not shown. (D) Overlay of the crystal structures of compound **6** (magenta) and (*S*)-**4** (yellow, PDB code 5ARG) showing nearly identical binding modes.

Figure 4. Comparison of (*S*)-**4** (this work) with the recently reported SMYD2 inhibitors **1**¹¹ and **2**.²⁵ (A) Chemical structures of the three selected SMYD2 inhibitors. (B) and (C) Two different views of an overlay of (*S*)-**4** (yellow) with **1** (green) and **2** (blue). (*S*)-**4** has a distinct binding mode, addressing pocket-2 which is not occupied by **1** or **2**, while only **1** and **2** occupy the distant hydrophobic pocket-3.

Figure 5. (*S*)-**4** mode of inhibition and selectivity profile. (A) Activity in the scintillation proximity assay (SPA). IC₅₀ (n > 10) for SMYD2 inhibition = 26 ± 7 nM (representative inhibition curve shown). (B) IC₅₀ values obtained from SPA were plotted against the indicated substrate concentrations (represented as [substrate]/K_{m(app)}). Data were fitted to competitive and uncompetitive models of the Cheng–Prusoff equation.^{41, 42} Data points are the mean of eight replicates, error bars indicate 1 × SD. The data indicate that (*S*)-**4** is a peptide-competitive, SAM-uncompetitive inhibitor of SMYD2 methyltransferase activity. (C) Selectivity profile on a panel of 32 additional methyltransferases showing high selectivity of (*S*)-**4** for SMYD2. Only SMYD3 is weakly inhibited by (*S*)-**4** with a > 1 μM IC₅₀.

Figure 6. Inhibition of cellular methylation of the tumor suppressor protein p53 by (*S*)-**4**. (A) A specific antibody directed against p53K370me1 (SY46) was generated and tested for specificity on recombinant p53 (rec. p53) which had been in vitro methylated by SMYD2, or non-methylated. (B) Endogenous methylation of p53 protein was characterized by treatment of KYSE-150 esophageal cancer cells with increasing concentrations of (*S*)-**4** for 5 days (Co =

control). (C) Cellular p53 methylation assay using transient FLAG-tagged SMYD2 and FLAG-tagged p53 overexpression in HEK293T cells. Increasing concentrations of (*S*)-**4** reduce the methylation of overexpressed p53 (for this assay p53K730me1-specific antibody kindly provided by Dr. Shelly Berger was used). (D) IC₅₀ determination in the cellular p53 methylation assay.

Figure 7. AHNAK is a novel substrate of SMYD2 and methylation can be inhibited by aminopyrazoline inhibitors. (A) In-Cell Western (ICW) assay. Immunofluorescence-based detection of AHNAK methylation. Each row represents a different inhibitor tested in increasing concentrations ranging from 39 nM up to 5 μ M. (*S*)-**4** and **1** are highlighted. (B) Inhibition of AHNAK methylation in MDA-MB231 cells overexpressing SMYD2. Methylation signal overlaps with AHNAK protein detection. (*S*)-**4** inhibits concentration dependent the AHNAK methylation (C) Good correlation of cellular activity (ICW) to biochemical activity (SPA) of (*S*)-**4** and pyrazoline cluster derivatives. (*S*)-**4** has a cellular IC₅₀ ~60 nM.

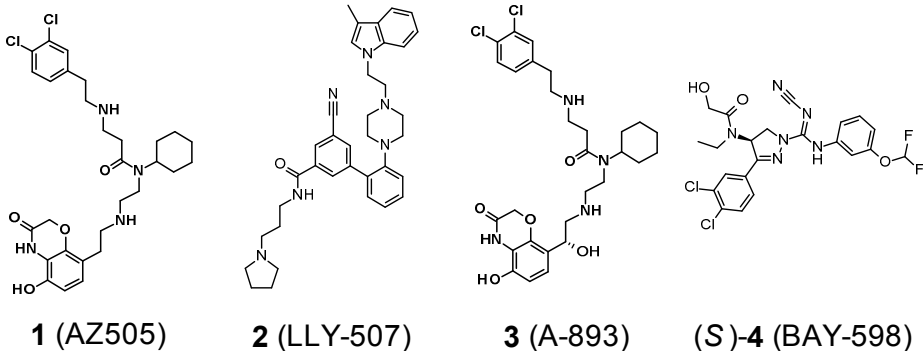
Figure 8. Proliferation and apoptosis effects of (*S*)-**4**. (A) A panel of 240 different cancer cell lines (OncoPanel 240/Eurofins Panlabs) was long-term cultured with (*S*)-**4** for 10 days and proliferation effects were determined. (*S*)-**4** showed proliferation effects with an IC₅₀ <10 μ M in a subset of cell lines. (B) Effects on apoptosis induction were determined by caspase 3/7 activation. KYSE-150, U2OS and A2780 cell lines were pre-treated with (*S*)-**4** or inactive derivative **25** (see Table 3) for 2 days, then apoptosis was induced by treatment with doxorubicin. (*S*)-**4**, but not **25**, significantly improved caspase 3/7 activation.

Figure 9. In vivo characterization of (*S*)-**4**. (A) Demethylation of AHNAK was evaluated ex vivo. Average methylation signals \pm standard deviation per group are shown. Mice (n = 12 per group) bearing subcutaneous tumor xenografts (tumor tissue derived from the SMYD2-

overexpressing KYSE-150 cell line) were treated as indicated, then the tumors were analyzed for methylation signals by dot-blotting. (S)-4 significantly reduced the methylation with doses starting from 30 mg/kg, with most significant effects in the 100 mg/kg group ($P < 0.001$, Student's t test). (B) Tumor area graph summarizing the in vivo tumor efficacy study with the KYSE-150 xenograft model. Average tumor area \pm standard error of mean per group is plotted as the mean. Treatment was started at day 4 after tumor inoculation (black arrow), and groups were treated as indicated. (C) Tumor weight graphs corresponding to the same experiment shown in (B). Average tumor weight are blotted as box plot. * Significant (p value < 0.05) difference between vehicle control and treatment group, (Dunn's method). Group 2: One animal was excluded on the 14th treatment day due to animal welfare reasons (ulcerated tumor), tumor size: 82 mm². (D) Mouse body weight analysis. Average body weight per group throughout the experiment is plotted as the mean.

Figures:

Figure 1



Reference	12	28	29	
Biochemical Activity				
Assay SMYD2 IC₅₀ [nM]	120 / 812	<15 / 388	2.8 / n.d.	27
(Reported / This Study)				
Mode of Action	substrate competitive	substrate competitive	substrate competitive	substrate competitive
Cellular Activity Assay				
IC₅₀ [nM]	<10,000 / 2900	600 / <1000	<10,000 / n.d.	58
(Reported / This study)				
In vivo PK				
Cl_B[L/h/kg] / F [%]	not reported	not reported	not reported	1.6 / 24

Figure 2

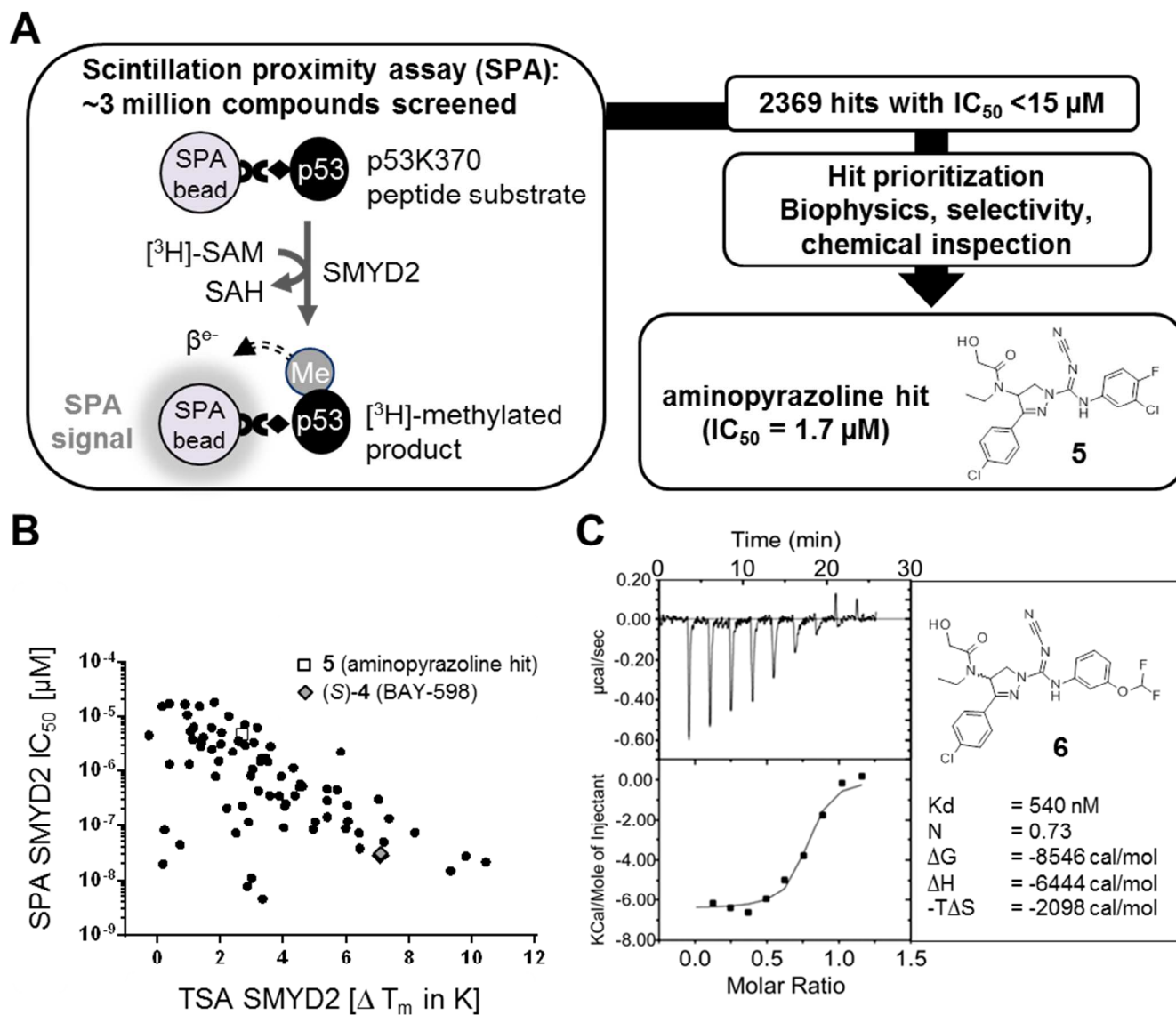


Figure 3

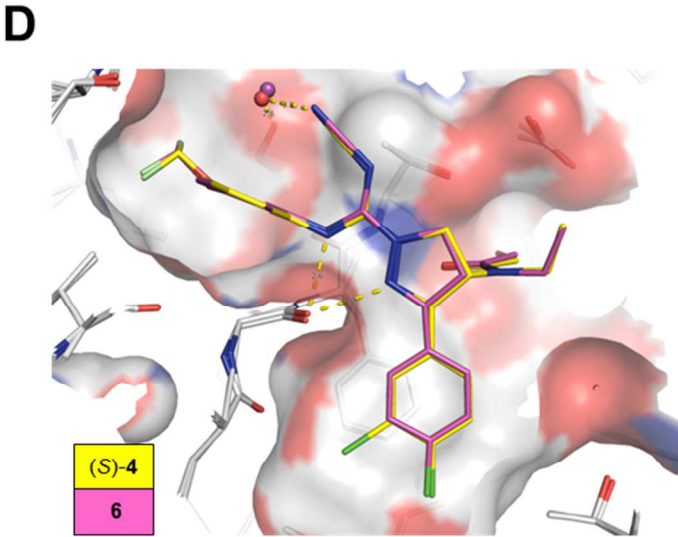
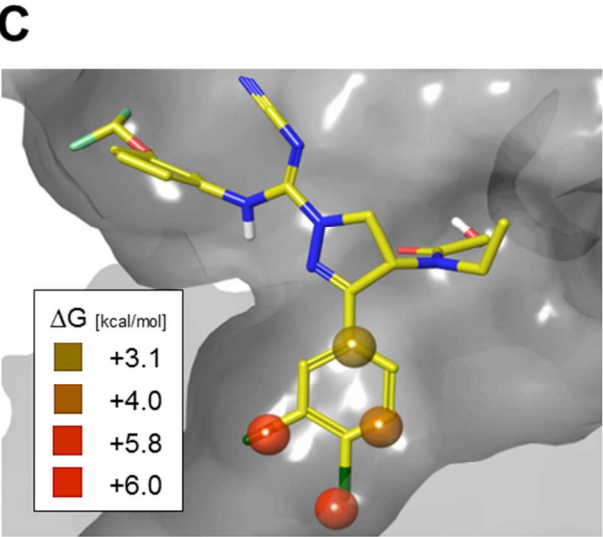
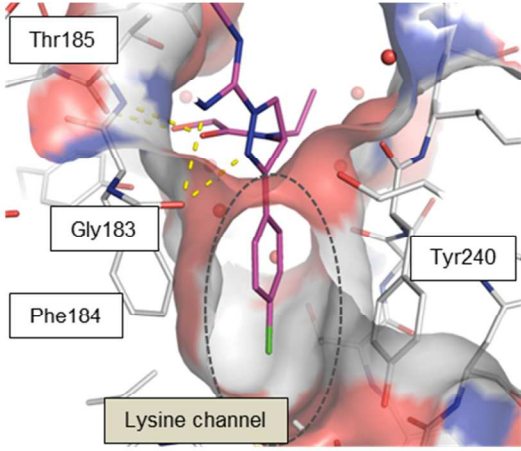
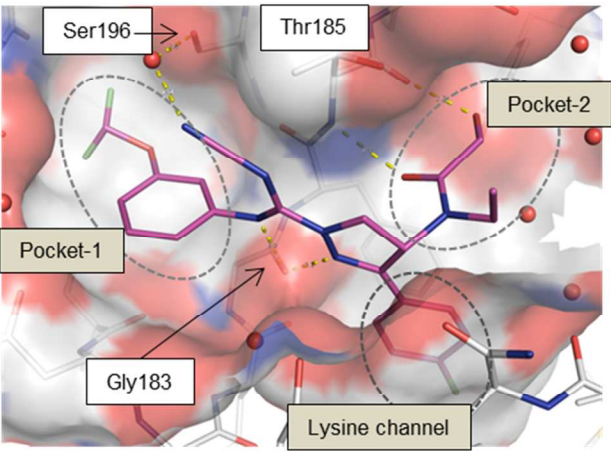


Figure 4

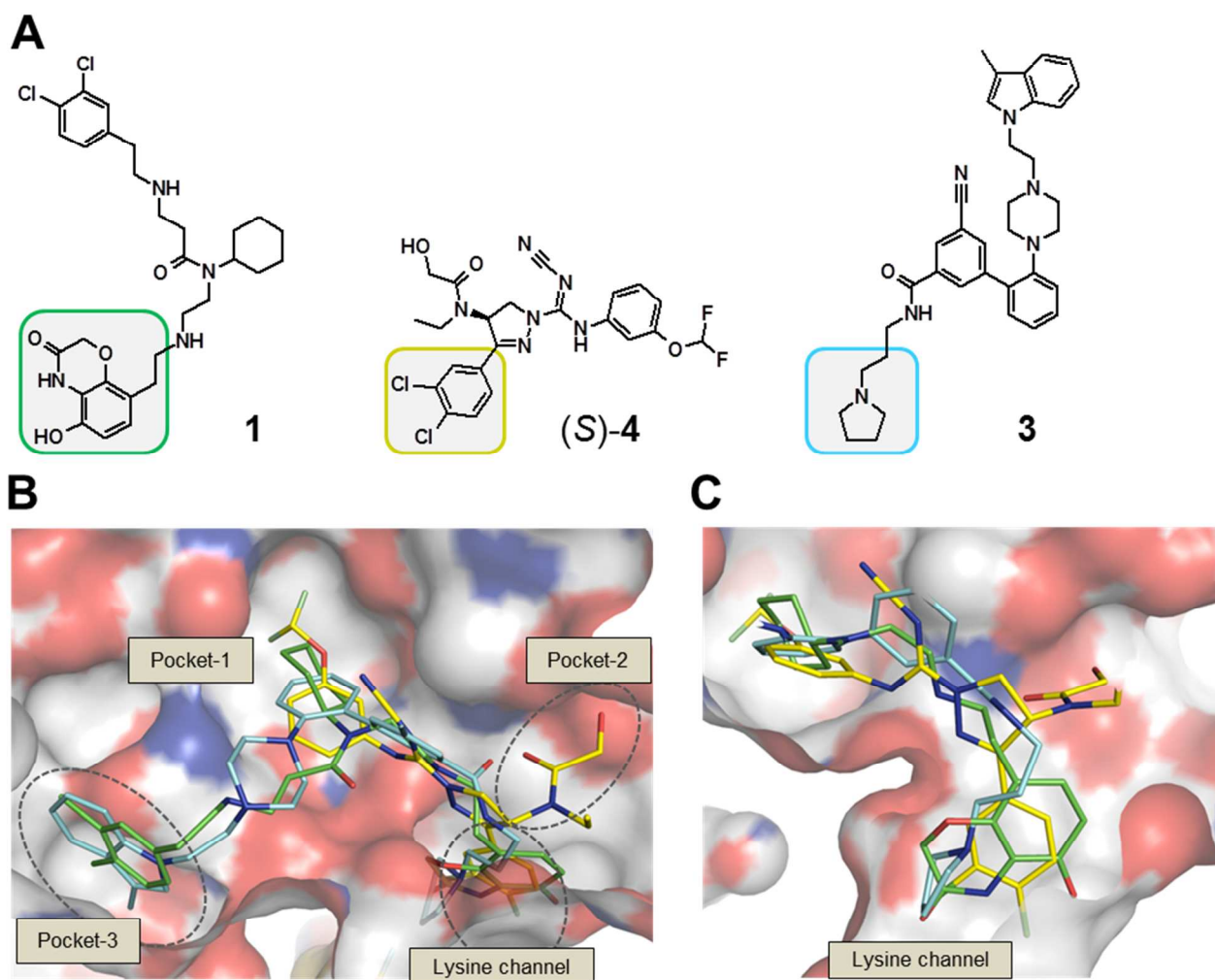


Figure 5

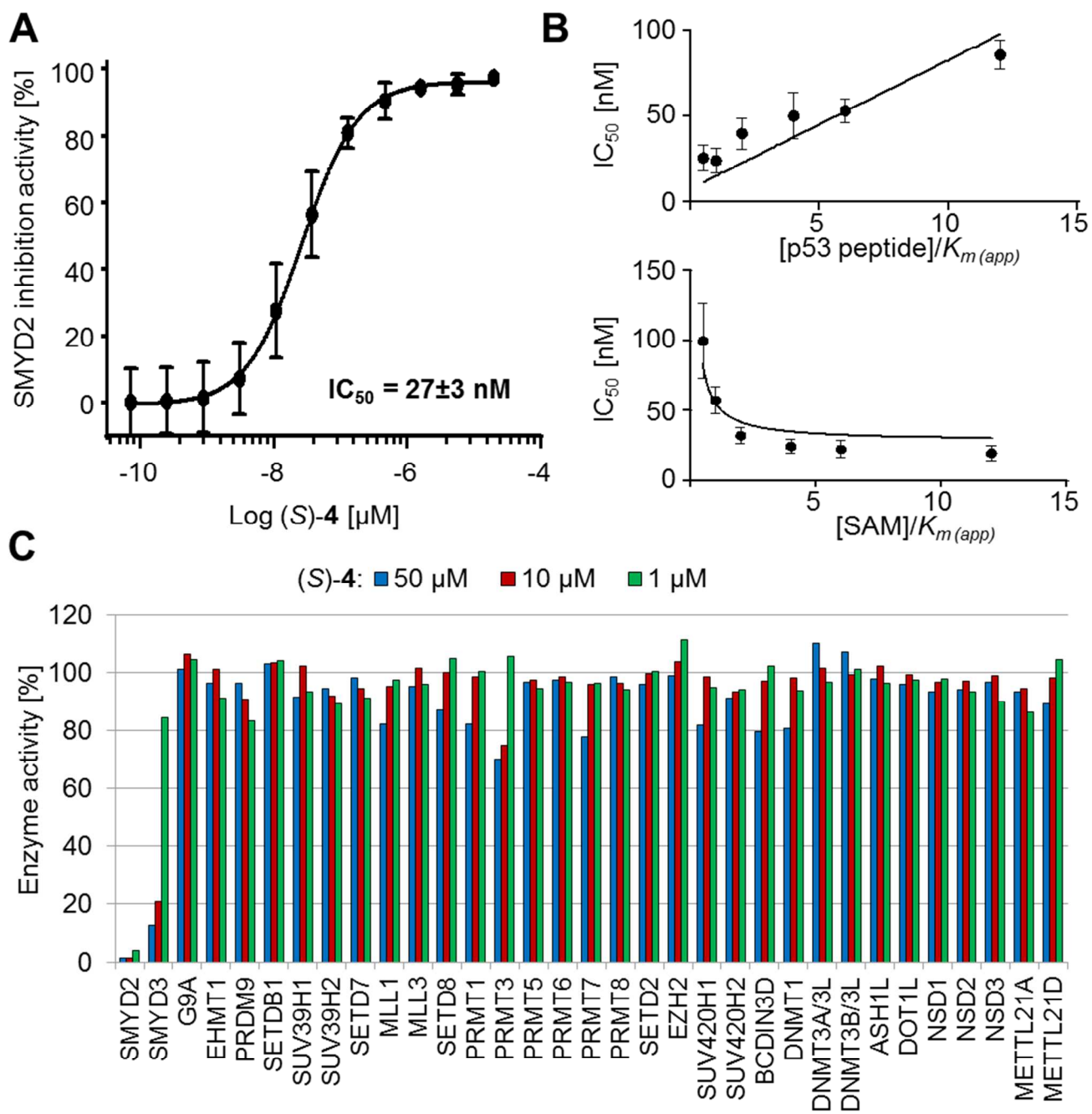


Figure 6

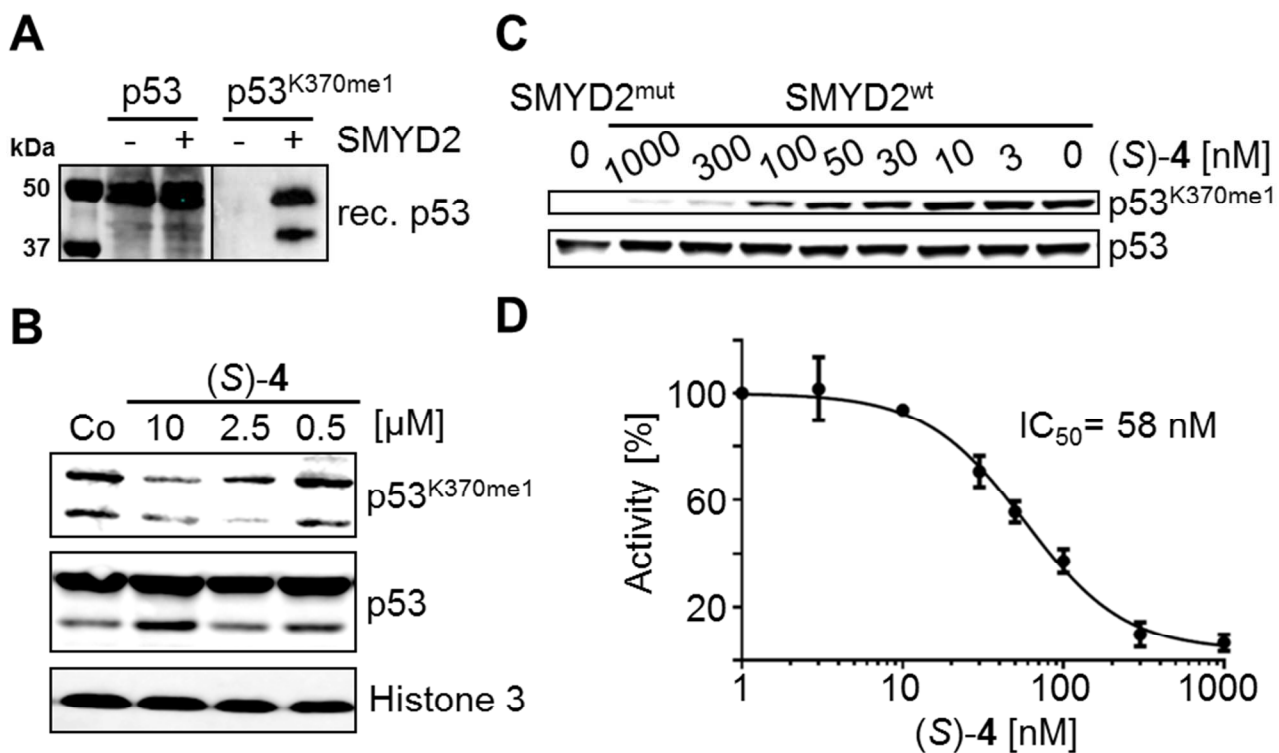


Figure 7

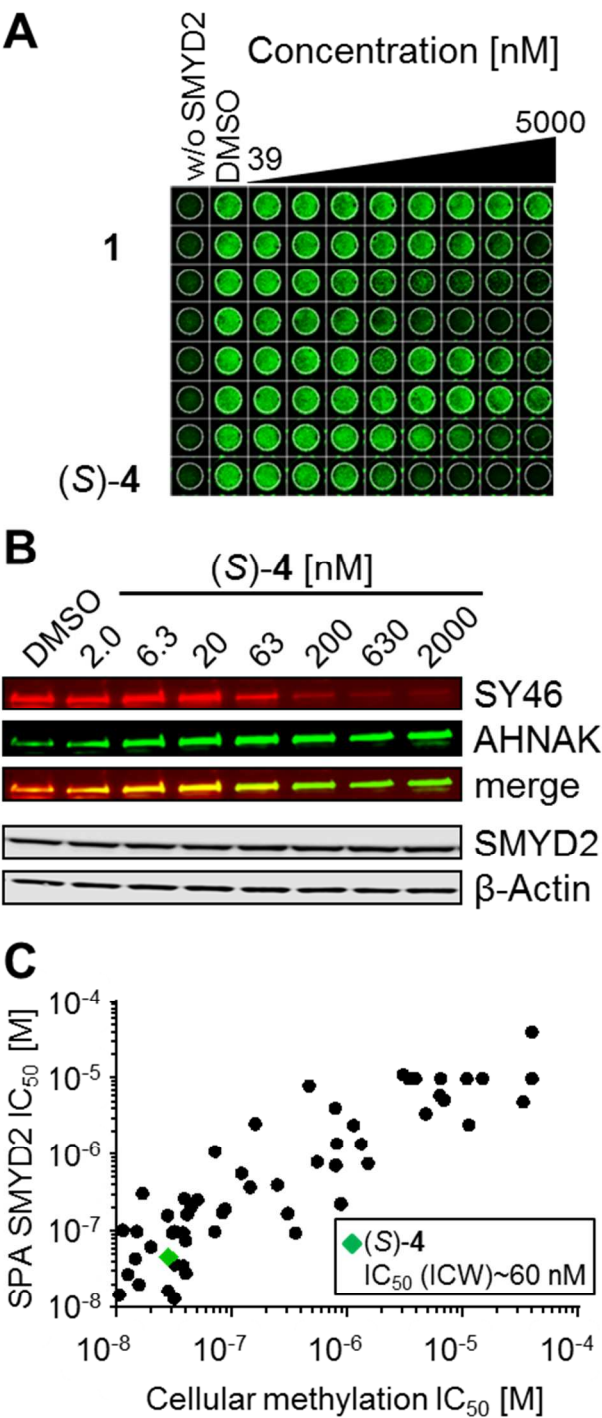


Figure 8

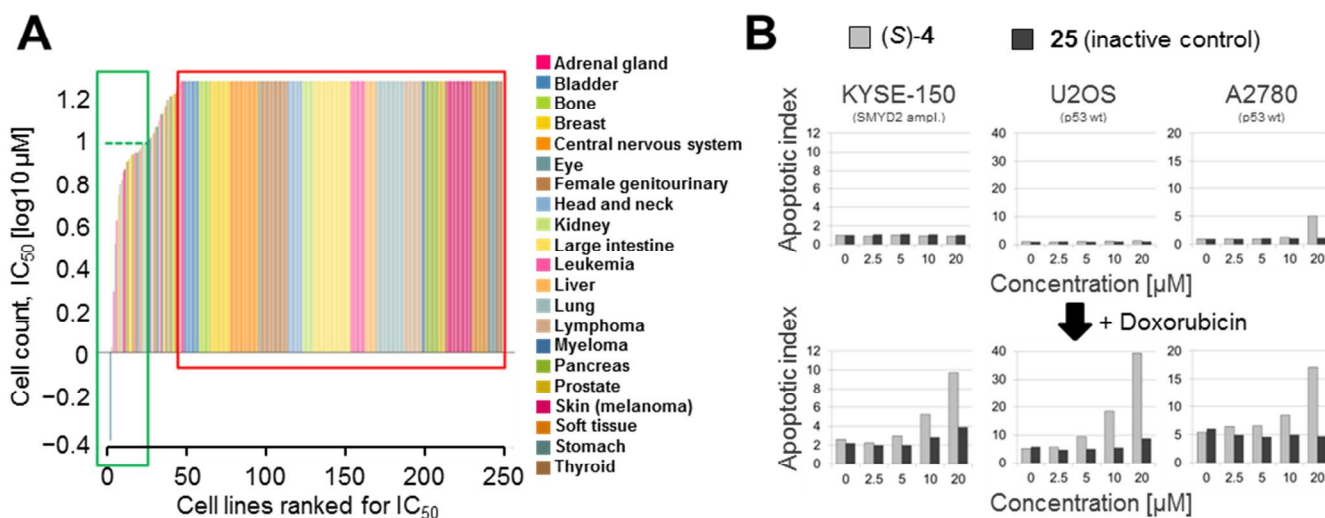
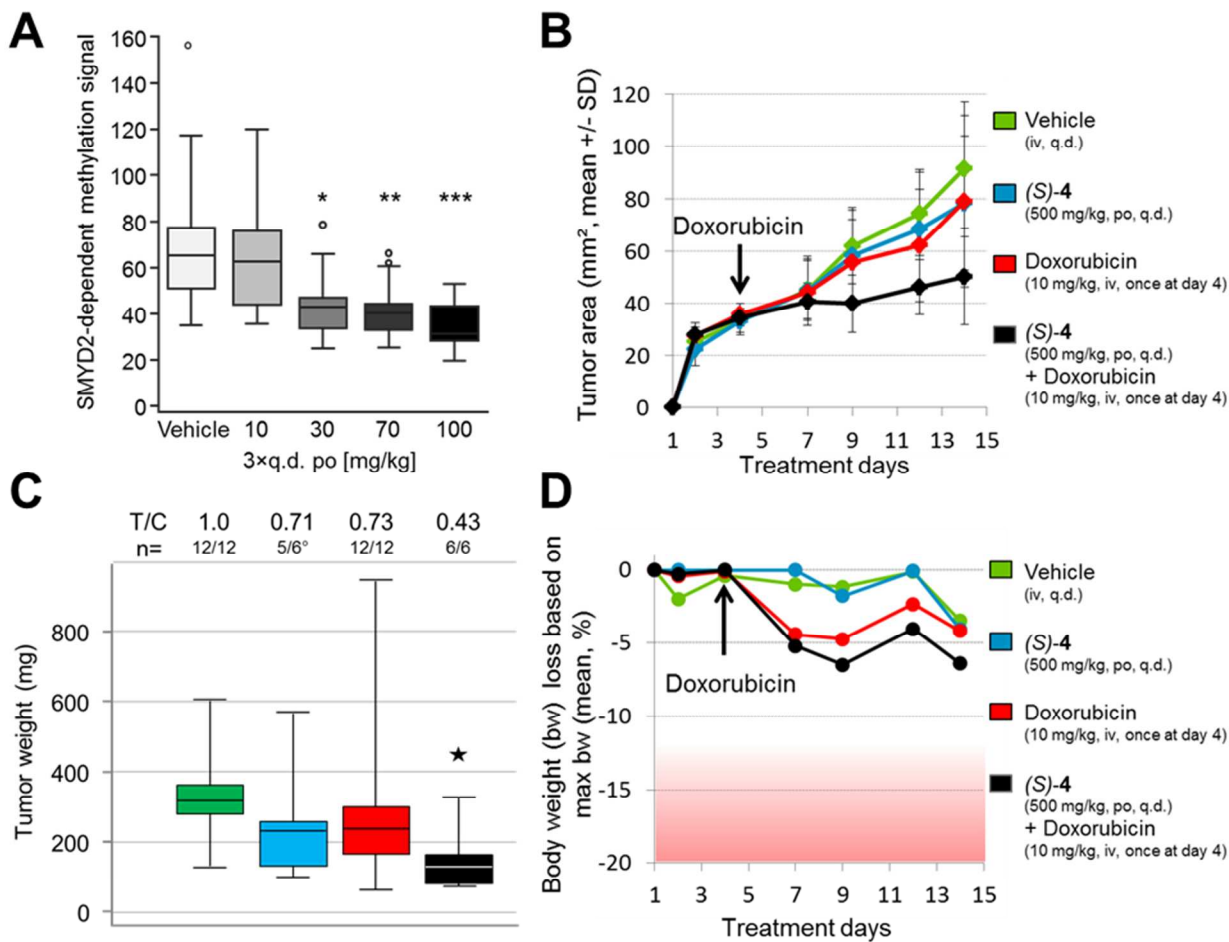


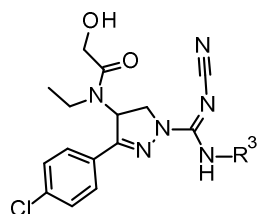
Figure 9



TABLES.

Table 1. SAR of 3-(4-Chlorophenyl)pyrazoline Derivatives: Variation of the Carboximidamide

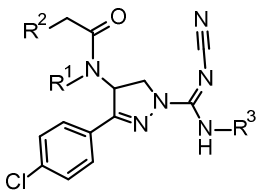
N-Substituent



Compound	R ³	SMYD2 IC ₅₀ [μM]	PAR1 IC ₅₀ [μM]	ΔT _m [K] ^a	BEI ^b (SMYD2)
5		1.7	0.06	3.3	12.1
6		0.8	0.07	3.4	12.5
12		3.3	0.05	2.4	11.1
13		2.2	0.08	3.8	11.2
14		15.8	0.06	0.9	9.8
15		>20	0.01	-0.4	—
16		6.9	0.05	2.7	11.3
17		>20	0.03	0.8	—
18		8.3	0.04	1.5	12.2

^aSMYD2 thermal shift assay. ^bBinding efficiency index: $pIC_{50}/MW \times 1000$.³⁸

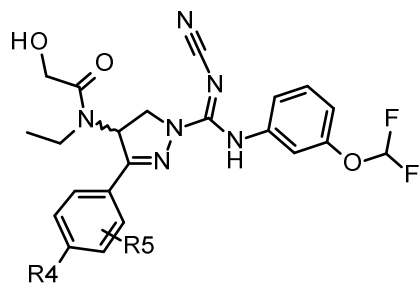
Table 2. SAR of 3-(4-Chlorophenyl)pyrazoline Derivatives: Variation of the Amide Moiety



Compound	R ¹	R ²	R ³	SMYD2 IC ₅₀ [μM]	PAR1 IC ₅₀ [μM]	ΔT _m [K] ^a	BEI ^b (SMYD2)
19	H	OH		10.9	—	1	10.7
20	<i>n</i> -Pr	OH		2.2	—	2.4	11.2
21		OH		>20	—	0.1	—
22	Et	NH ₂		2.8	0.13	3.8	11.3
23	Et	OMe		>20	0.03	0.7	—
24				6	0.1	2.2	11

^aSMYD2 thermal shift assay. ^bBinding efficiency index: $pIC_{50}/MW \times 1000$.³⁸

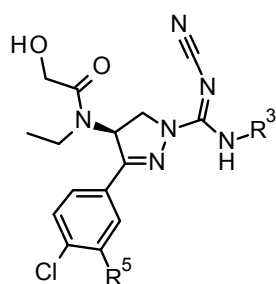
Table 3. SAR of 3-Phenylpyrazoline Derivatives: Exploration of Phenyl Substituents



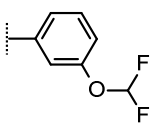
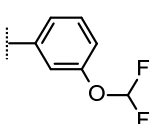
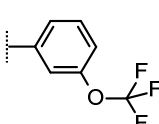
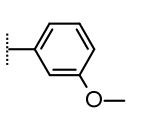
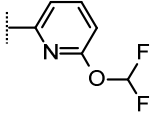
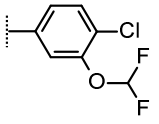
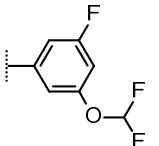
Compound	R ⁴	R ⁵	SMYD2 IC ₅₀ [μM]	Δ <i>T</i> _m ^a [K]	BEI ^b
25	H	H	>20	0.6	–
26	Br	H	1.1	4.3	11.1
27	Cl	3,5-Me ₂	0.57	3.0	12
4	Cl	3-Cl	0.08	–	13.5
28	Cl	3-Me	0.08	4.9	14
29		OCH ₂ O	4.2	0.3	10.7

^aSMYD2 thermal shift assay. ^bBinding efficiency index: pIC₅₀/MW × 1000.³⁸

Table 4. In Vitro Pharmacokinetic Properties of Potent SMYD2 Inhibitors



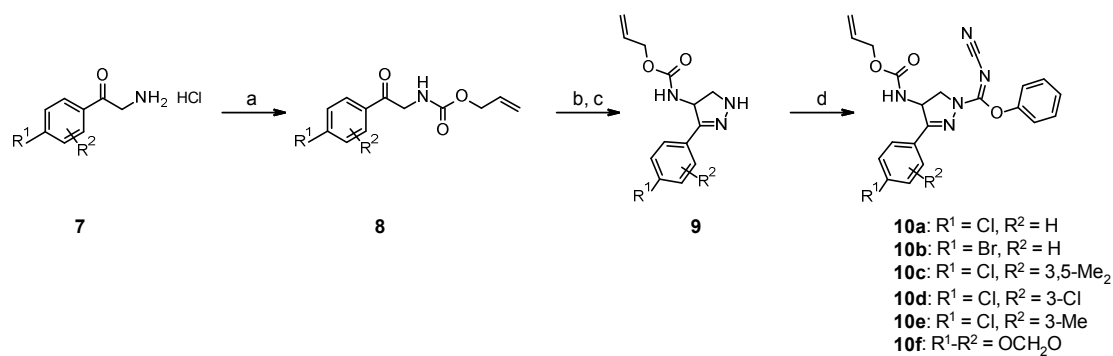
Compound ^a	R ³	R ⁵	SMYD2 IC ₅₀ [μM]	PAR1 IC ₅₀ [μM]	CL ^b [L/h/kg]	Caco2 ^c [nm/s]	Sol. ^d [mg/L]
(<i>S</i>)- 4 (BAY-598)		Cl	0.027	1.7	2.5	34/5	20

(R)-4		Cl	1.7	>30	–	–	11
(S)-28		Me	0.038	–	2.8	33/7	<1
(S)-30		Cl	0.05	–	1.6	32/2	3
(S)-31		Cl	0.071	–	3.2	62/3	163
(S)-32		Cl	0.119	–	1.8	39/4	3
(S)-33		Cl	0.044	–	1.4	10/10	<1
(S)-34		Cl	0.019	–	0.3	23/6	<1

^aee > 95 %. ^bRat hepatocytes. ^cPermeability $P_{app}(A-B)$ /efflux ratio. ^dAqueous solubility.

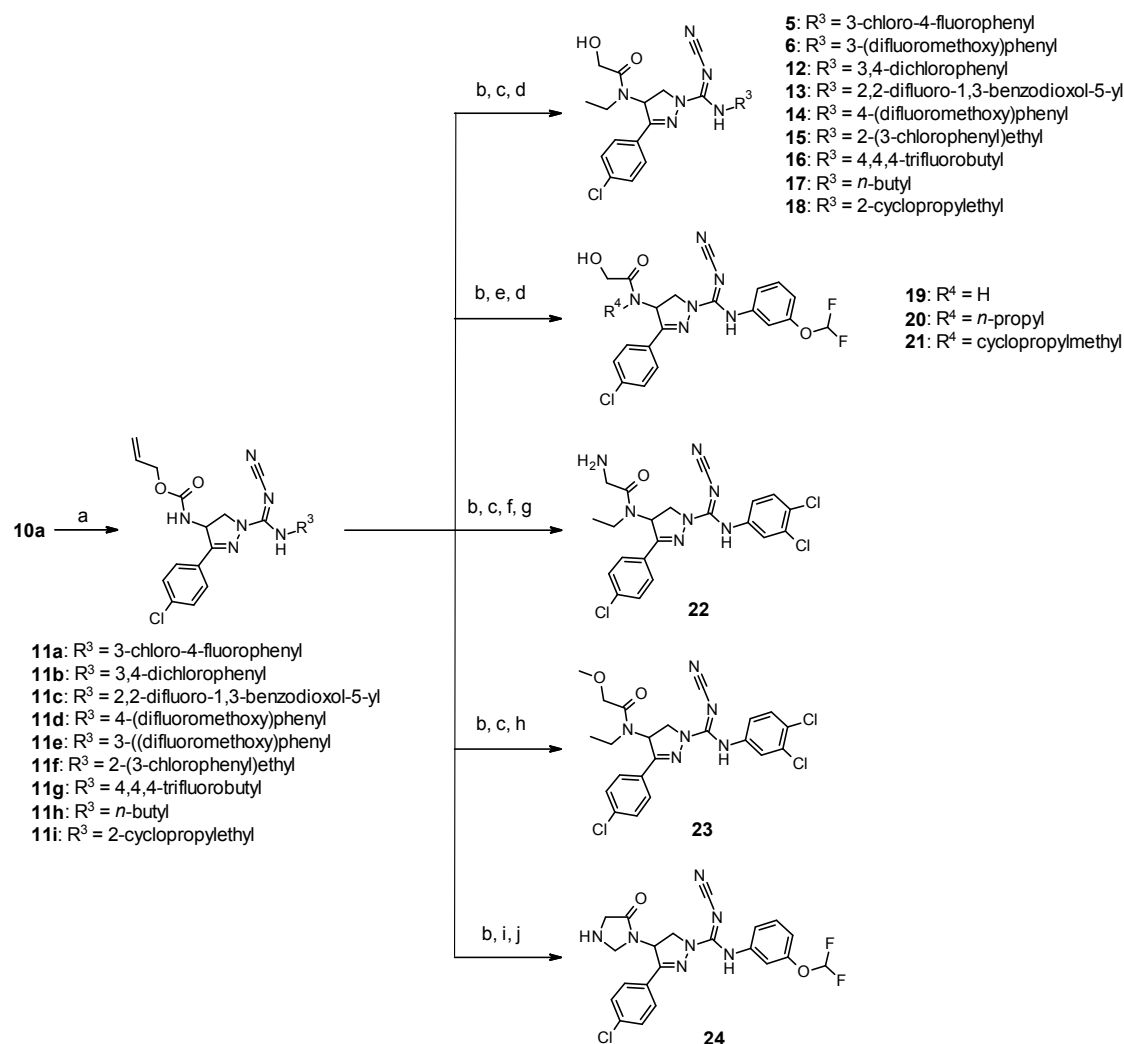
SCHEMES.

Scheme 1. Synthesis of Pyrazoline Intermediates **10a–f**^a



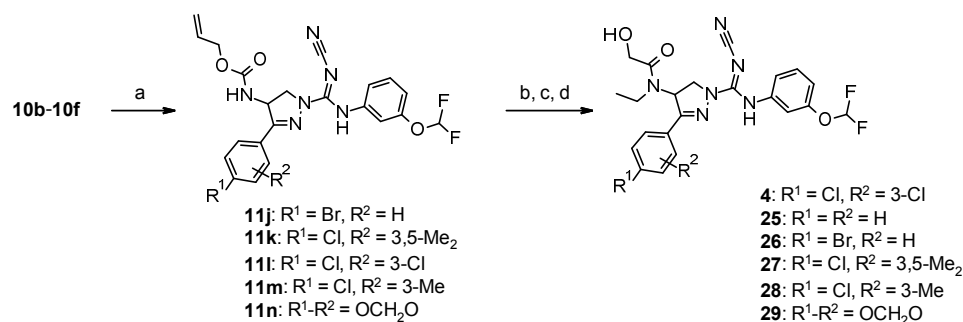
"Reagents and conditions: (a) allyl chloroformate, K_2CO_3 (1.5 M in water), DCM, rt, overnight. (b) formaldehyde (37 wt% in water), piperidine, EtOH, rt, overnight. (c) hydrazine monohydrate, EtOH, reflux. (d) diphenyl *N*-cyanocarbonimidate, *i*-PrOH, reflux, 1 h, then rt, overnight.

Scheme 2. Synthesis of Compounds 5, 6 and 12–24^a



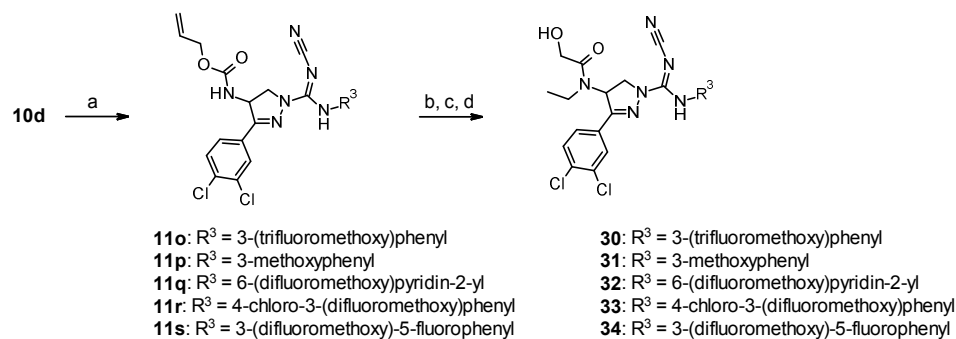
“Reagents and conditions: (a) aniline derivative, *n*-BuLi, THF, $-78\text{ }^{\circ}\text{C}$; or alkylamine, 1,4-dioxane, reflux. (b) 1,3-dimethylbarbituric acid, $\text{Pd}(\text{PPh}_3)_4$, THF. (c) acetaldehyde, NaBH_4 , DCM, $0\text{ }^{\circ}\text{C}$. (d) (1) acetoxyacetyl chloride, aqueous NaHCO_3 solution, DCM; (2) K_2CO_3 , MeOH. (e) skip (for compound **19**), or aldehyde derivative, NaBH_4 , MeOH, $0\text{ }^{\circ}\text{C}$. (f) Fmoc-glycine, HATU, NMM, DMF. (g) piperidine, DMF. (h) methoxyacetyl chloride, aqueous NaHCO_3 solution, DCM. i) chloroacetyl chloride, *N,N*-diisopropylethylamine, DCM. (j) urotropine, EtOH.

Scheme 3. Synthesis of Compounds **4** and **25–29**^a



“Reagents and conditions: (a) 3-(difluoromethoxy)aniline, *n*-BuLi, THF, $-78\text{ }^{\circ}\text{C}$. (b) 1,3-dimethylbarbituric acid, $\text{Pd}(\text{PPh}_3)_4$, THF. (c) acetaldehyde, NaBH_4 , MeOH, $0\text{ }^{\circ}\text{C}$. (d) (1) acetoxyacetyl chloride, aqueous NaHCO_3 solution, DCM; (2) K_2CO_3 , MeOH.

Scheme 4. Synthesis of Compounds **30–34**^a



“Reagents and conditions: (a) aniline derivative, *n*-BuLi, THF, $-78\text{ }^{\circ}\text{C}$. (b) 1,3-dimethylbarbituric acid, $\text{Pd}(\text{PPh}_3)_4$, THF. (c) acetaldehyde, NaBH_4 , MeOH, $0\text{ }^{\circ}\text{C}$. (d) (1) acetoxyacetyl chloride, aqueous NaHCO_3 solution, DCM; (2) K_2CO_3 , MeOH.

1
2
3
4
5
6
7
8
9
10
11
12
13
14
15
16
17
18
19
20
21
22
23
24
25
26
27
28
29
30
31
32
33
34
35
36
37
38
39
40
41
42
43
44
45
46
47
48
49
50
51
52
53
54
55
56
57
58
59
60

TABLE OF CONTENTS GRAPHIC

